Vol. 92 No. 4 pp. 1349–1365 ACTA GEOLOGICA SINICA (English Edition) Aug. 2018

# Early-Cretaceous Syenites and Granites in the Northeastern Tengchong Block, SW China: Petrogenesis and Tectonic Implications

ZHU Renzhi, LAI Shaocong*, QIN Jiangfeng and ZHAO Shaowei

*State Key Laboratory of Continental Dynamics, Department of Geology, Northwest University, Xi'an 710069, China*

**Abstract: Whole-rock major and trace element and Sr-Nd isotopic data, together with zircon LA ICP-MS in-situ U-Pb and Hf isotopic data of the syenites and granites in the Tengchong Block are reported in order to understand their petrogenesis and tectonic implications. Zircon U-Pb data gives the emplacement ages of ca. 115.3±0.9 Ma for syenites and 115.7±0.8 Ma for granites, respectively. The syenites are characterized by low $SiO_2$ content (62.01–63.03 wt%) and notably high $Na_2O$ content (7.04–7.24 wt%) and $Na_2O/K_2O$ ratios (2.02–2.10), low MgO, $Fe_2O_3T$ and $TiO_2$, enrichment of LILEs(large-ion lithophile element) such as Rb, Th, U, K, and Pb) and obvious depletion HFSE(high field strength element; e.g. Nb, Ta, P, and Ti) with clearly negative Eu anomalies (*d*Eu=0.53–0.56). They also display significant negative whole-rock $\varepsilon$Nd(*t*) values of −6.8 and zircon $\varepsilon$Hf(*t*) values(−9.11 to −0.27, but one is +5.30) and high initial $^{87}Sr/^{86}Sr$=0.713013. Based on the data obtained in this study, we suggest that the ca. 115.3Ma syenites were possibly derived from a sodium-rich continental crustal source, and the fractionation of some ferro-magnesian mineral and plagioclase might occur during the evolution of magma. The granites have high $SiO_2$ content (71.35–74.47 wt%), metaluminous to peraluminous, low Rb/Ba, Rb/Sr, and $Al_2O_3$/(MgO+FeOT+$TiO_2$) ratios and moderate ($Al_2O_3$+MgO+FeOT+$TiO_2$) content. They show low initial $^{87}Sr/^{86}Sr$ (0.703408 to 0.704241) and $\varepsilon$Nd(*t*) values (−3.8 to −3.5), plotted into the evolutionary trend between basalts and lower crust. Hence, we suggest that the granites were derived from the melting of mixing sources in the ancient continental crust involving some metabasaltic materials and predominated metasedimentary greywackes. Together with data in the literatures, we infer that the Early Cretaceous magmatism in the Tengchong block was dominated by magmas generated by the partial melting of ancient crustal material, which represent the products that associated to the closure of Bangong-Nujiang Meso-Tethys.**

**Key words: Early Cretaceous, syenite, granite, crustal sources, Tengchong Block**

## 1 Introduction

Granites are widespread in the upper crust, especially in orogenic belts, and an understanding of their genesis provides insight into the evolution of their deep continental source and tectonic setting (Chappell and White, 1992; Sylvester, 1998; Brown, 2013; Hao et al., 2015; Zhang et al., 2015; Wu et al., 2015), such as subduction, collision, or post-orogenic extension. Meanwhile, syenites are also an important objects to decipher the magmatic processes within the continental lithosphere such as the sources in the lower and upper crust (Chen et al., 2017; Yang et al., 2012), which were usually been proposed as the products of: (1) partial melting of crustal rocks (Huang and Wyllie, 1975; Lubala et al., 1994); (2) differentiation of mantle-derived mafic rocks (Litvinovsky et al., 2002; Yang et al., 2005); (3) differentiation of the hybrid liquids (mixing between basic and silicic melts or mantle-derived silica-undersaturated alkaline magmas with lower crustal-derived granitic magmas) (Sheppard, 1995; Dorais, 1990; Riishuus et al., 2005; Yang et al., 2008). In contrast to granites, it is commonly developed in the extensive setting including including post-orogenic, rift, or intraplate tectonic setting (Sylvester, 1989; Bonin et al., 1998; Yang et al., 2005; Yang et al., 2012 reference therein). Therefore, the petrogenesis of both syenites and granites are crucial to understand the magmatic process and deep sources in the continental crust.

In our recent field investigations, some Early-

* Corresponding author. E-mail: shaocong@nwu.edu.cn

Cretaceous syenites and granites are found out in the Qushijie and Lushui area in the northeastern Tengchong Block, we all know that the abundant Early-Cretaceous magmatism in the Tengchong block was related to the subducted and closure process of the Bangong-Nujiang Meso-Tethyan ocean (Xu et al., 2012; Zhu et al., 2015b; Zhu et al., 2017a, b). Hence, we present the zircon LA ICP -MS U-Pb data, whole-rock chemical and Sr-Nd isotopic data, and zircon in-situ Hf isotopic data to constraint the petrogenesis of the syenites and granites, which aim to understand the continent crustal magmatic processes and deep sources during the subducted and closure process of Bangong-Nujiang Tethyan ocean.

## 2 Geological Setting and Petrography

The Tengchong Block represents the southeastern extension of the Lhasa Block (Xie et al., 2016; Fig. 1a) and is separated from the eastern Baoshan Block by the Nujiang–Luxi–Ruili fault (NLRF) and from the western Burma Block by the Putao–Myitkyina suture zone (Li et al., 2004; Cong et al., 2011a and b; Xu et al., 2012; Wang et al., 2013; Metcalfe, 2013). Based on the presence of Permo-Carboniferous glacio-marine deposits and overlying post-glacial black mudstones and Gondwana-like fossil assemblages, it has been suggested that the Tengchong Block was derived from the margins of

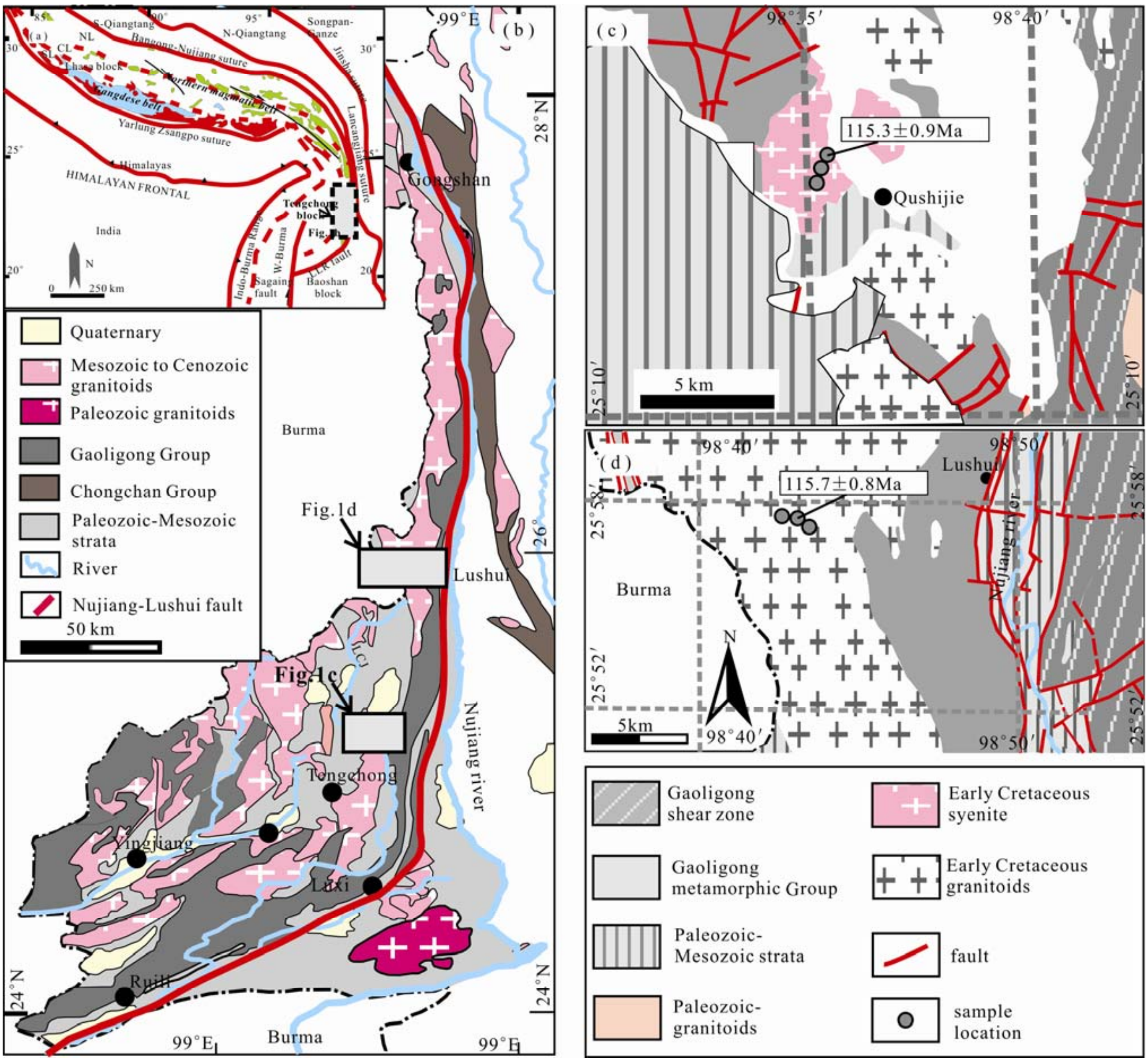

Fig. 1. (a), distribution of main continental blocks of SE Asia (Xu et al., 2012). (b), the magmatic distribution in the Tengchong Block (Zhu et al., 2017b). (c), distribution of the syenites near Qushijie in the northern part of Menglian batholiths (YNBGMR, 1991). (d), Study area of the granitic rocks in the northeastern of Tengchong block (YNBGMR, 1991).

western Australia, in the eastern part of the Gondwana supercontinent (Jin, 1996). The block contains Mesoproterozoic metamorphic basement belonging to the Gaoligong Mountain Group and upper Paleozoic clastic sedimentary rocks and carbonates. The Mesozoic to Tertiary granitoids were emplaced into these strata and were then covered by Tertiary–Quaternary volcano-sedimentary sequences (YNBGMR, 1991). The Gaoligong Mountain Group contains quartzites, two-mica–quartz schists, feldspathic gneisses, migmatites, amphibolites, and marble. Zircons from the paragneiss and orthogneiss samples in this group yield ages in the range of 1053–635 and 490–470 Ma, respectively (Song et al., 2010). The Paleozoic sediments in this area are dominated by Carboniferous clastic rocks, and others Mesozoic strata including Upper Triassic to Jurassic turbidites, Cretaceous red beds, and Cenozoic sandstones (YNBGMR, 1991; Zhong Dalai, 2000).

The Tengchong Block contains abundant granitic gneiss, migmatite, and leucogranite units, the vast majority of which were previously thought to have formed during the Proterozoic (YNBGMR, 1991). However, recent studies have identified several massive granitoids with zircon U–Pb ages of 114–139 Ma in the eastern part of this block (Yang et al., 2006; Cong et al., 2011a and b; Xie et al., 2010; Qi et al., 2011; Li et al., 2012; Luo et al., 2012; Xu et al., 2012; Cao et al., 2014; Zhu et al., 2015b; Xie et al., 2016), all of which were emplaced into the Paleozoic and Mesozoic units. The granites in the Gaoligong area are located to the west of the Nujiang–Luxi–Ruili fault and have undergone strong shearing that developed a north-trending foliation and a subhorizontally plunging mineral lineation (Wang and Burchfiel, 1997; Zhang et al., 2012).

This study focuses on the syenite from Menglian batholiths and granite from the Gaoliogong belt of the northeastern part of Tengchong block (Fig. 1b and c; Table 1). The Menglian batholith are located in the eastern Tengchong Terrane and intruded into the Gaoligong Group metamorphic rocks as well as the Paleozoic-Mesozoic strata (Fig. 1b). In most cases, they show faulted contact with the wall-rock although the intrusive contact can be seen in some places as well. Cenozoic volcanic rocks unconformably overly these intrusions and/or are covered by Quaternary sediments (Luo et al. 2012). The intrusions show round or elongate shape, and occur parallel to the ~NNW–SSW orientation with the Gaoligong shear zone and Nujiang-Longling-Ruili fault (NLRF) which are regarded to mark the southeastern extension of the Nujiang suture belt (Cong et al., 2011a). The studied pluton was located on the northern of the Menglian batholith near the Qushijie town, which mainly consists of the syenites that as the intrusions in the Paleozoic-Mesozoic strata and Gaoligong Group metamorphic rocks with sharply and unconformably contact (Fig. 1b). The syenite are medium to coarse grain and some part porphyroid texture and massive structure (Fig. 2a), mainly contained of plagioclase (most of them are albite, 50–55 %), alkaline feldspar (15–20 vol%), quartz (5–10 vol%), hornblend (possible arfvedsonite, 5–10 vol%), biotite (5 vol%), and accessory mineral including titanite, magnetite, zircon, and apatite (Fig. 2b).

Then, the N-S trending granites in the Gaoligong belt are less deformed, extends northward into the NWW-trending Bomi-Chayu (TransHimalaya) magmatic belt. It was also extended south-westward into the Tengchong-Lianghe-Yingjiang area, and likely extends further into the Shan Scarp in Burma. The basement in the Gaoligong area is also composed of flat foliated granites and metamorphic rocks. The Gaoligong granites are intruded into the Precambrian Gaoligong Group, massive structure in the middle but slightly mylonitization occurred in the eastern and western margin. It was exposed as the long and narrow lens between the Nujiang and Longchuanjiang strike-slip faults and characterized by the obviously syntectonic emplacement (Fig. 1c). The granites are medium grained and also massive structure (Fig. 2c), and mainly consist of alkaline feldspar (25–40 vol%), plagioclase (18–25 vol%), quartz (25–33 vol%), biotite (10–12 vol%), amphibole (1vol%), and accessory minerals including sphene, zircon, and apatite (Fig. 2d).

## 3 Samples and Analytical Methods

### 3.1 Major and trace elements

Whole-rock samples were trimmed to remove weathered surfaces, cleaned with deionized water, crushed, and then powdered through a 200 mesh screen using a tungsten carbide ball mill. Major elements were analyzed using an X-ray fluorescence (XRF) spectrometer (Rikagu RIX 2100) at the Guizhou Tuopu Resource and Environmental Analysis Center, Institute of Geochemistry,

**Table 1 Summary of petrological characters of the Early-Cretaceous syenite-granites in the Tengchong Block**

| Sample | Location | Petrology | Age (Ma) | Structure | Minerals |
|---|---|---|---|---|---|
| DMJ13 | N: 25°16.056'<br>E:98°35.525' | syenite | 115.3±0.87 | medium to coarse grain;<br>some part porphyroid texture; massive structure | Pl(50–55%)+Kf(15–20%)+Qtz(5–10%)+<br>Hbl(5–10%)+Bt(5%) |
| PM2-100 | N:25°57.738'<br>E:98°42.948' | granite | 115.7±0.77 | medium grained;<br>massive structure | Pl(18–25%)+Kf(25–40%)+Qtz(25–33%)+<br>Hbl(1%)+Bt(10–12%) |

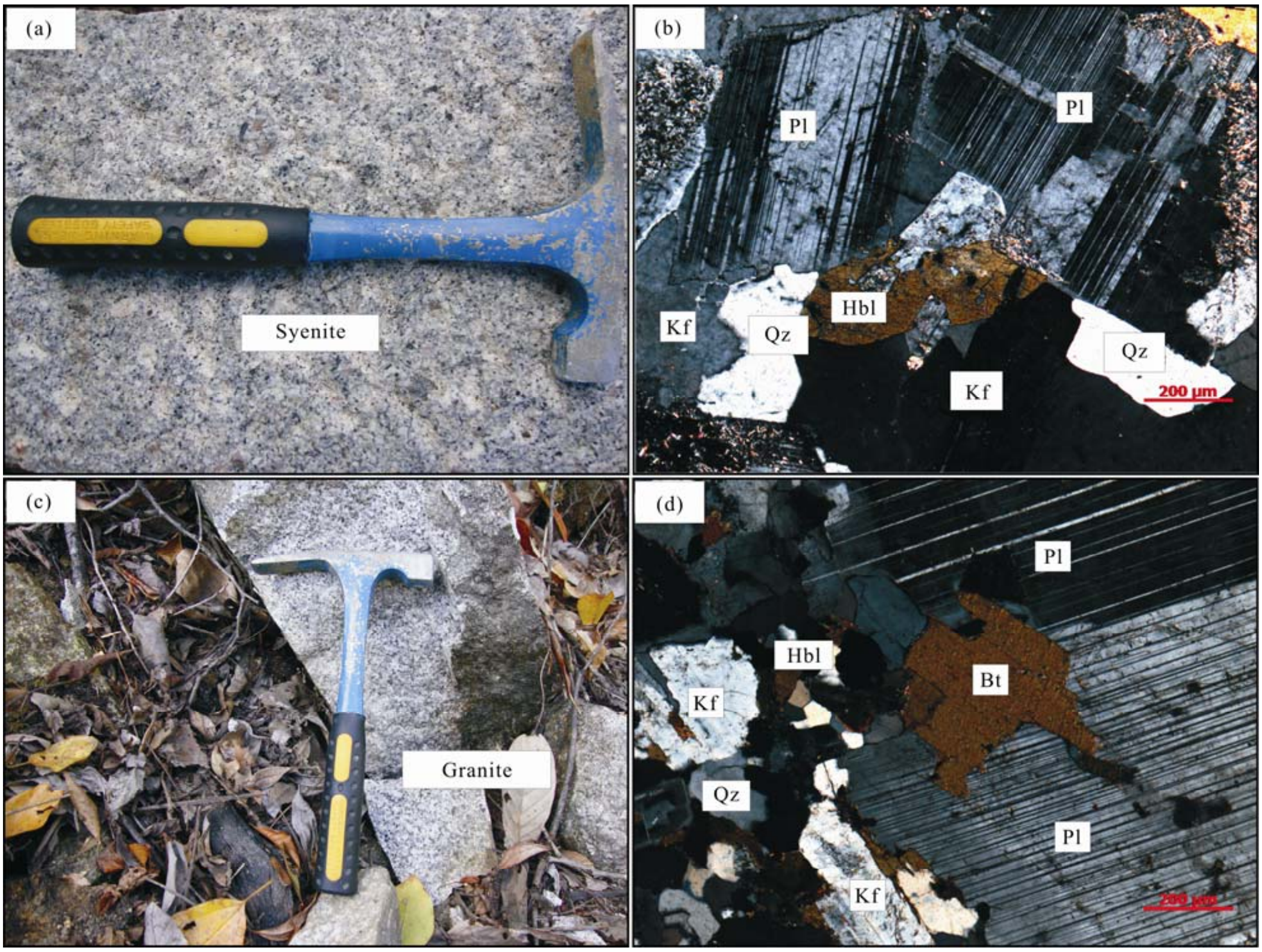


Fig. 2. Field and petrological features of syenites and granites in the Tengchong block, SW China.

Chinese Academy of Sciences, Guiyang, China. Analyses of USGS and Chinese national rock standards (BCR-2, GSR-1, and GSR-3) indicate that both analytical precision and accuracy for major elements are generally better than 5%. Trace elements were determined by using a Bruker Aurora M90 inductively coupled plasma mass spectrometry (ICP-MS) at the Guizhou Tuopu Resource and Environmental Analysis Center, Institute of Geochemistry, Chinese Academy of Sciences, Guiyang, China. Following the method of Qi et al. (2000). Sample powders were dissolved using an $HF+HNO_3$ mixture in a high-pressure PTFE bomb at 185°C for 36 h. The accuracies of the ICP-MS analyses are estimated to be better than ±5–10% (relative) for most elements.

### 3.2 Sr–Nd isotopic analyses

Whole-rock Sr–Nd isotopic data were obtained by using a Nu Plasma HR multi-collector mass spectrometer at the State Key Laboratory of Continental Dynamics, Northwest University, China. The Sr and Nd isotopes were determined by using a method similar to that of Chu et al. (2009). Sr and Nd isotopic fractionation was corrected to $^{87}Sr/^{86}Sr$=0.1194 and $^{146}Nd/^{144}Nd$=0.7219, respectively. During the period of analysis, a Neptune multi-collector ICP-MS was used to measure the $^{87}Sr/^{86}Sr$ and $^{143}Nd/^{144}Nd$ isotope ratios. NIST SRM-987 and JMC-Nd were used as certified reference standard solutions for $^{87}Sr/^{86}Sr$ and $^{143}Nd/^{144}Nd$ isotopic ratios, respectively. BCR-1 and BHVO-1 were used as the reference materials.

### 3.3 Zircon U–Pb and Hf isotopic analyses

Zircon was separated from three ~5 kg samples taken from various sampling locations within the Gaoligong belt. The zircon grains were separated by using conventional heavy liquid and magnetic techniques. Representative zircon grains were handpicked and mounted in epoxy resin disks and then polished and coated with carbon. Internal morphology was examined using cathodoluminescent (CL) prior to U–Pb analyses.

Laser ablation ICP-MS zircon U–Pb analyses were conducted on an Agilent 7500a ICP-MS equipped with a 193-nm laser, which is housed at the State Key Laboratory of Continental Dynamics, Northwest University, Xi'an, China, following the method of Yuan et al. (2004). The $^{207}Pb/^{206}Pb$ and $^{206}Pb/^{238}U$ ratios were calculated by using the GLITTER program and corrected using the Harvard zircon 91500 as external calibration. These correction factors were then applied to each sample to correct for both instrumental mass bias and depth-dependent elemental and isotopic fractionation. The detailed analytical technique is described in Yuan et al. (2004). Common Pb contents were therefore evaluated by using the method described in Andersen (2002). The age calculations and plotting of concordia diagrams were made using ISOPLOT (version 3.0) (Ludwig, 2003). The errors quoted in tables and figures are at the 2σ level.

In situ zircon Hf isotopic analyses were conducted using a Nepyune MC-ICPMS, equipped with a 193nm laser. During analyses, a laser repetition rate of 10Hz at 100 Mj was used and spot sizes were 32 μm. During analyses, $^{176}Hf/^{177}Hf$ and $^{176}Lu/^{177}Hf$ ratios of the standard zircon (91500) were 0.282294±15 (2σ, n=20) and 0.00031, similar to the commonly accepted $^{176}Hf/^{177}Hf$ ratio of 0.282302±8 and 0.282306±8 (2σ) measured using the solution method (Goolaerts et al., 2004). The notations of $\varepsilon Hf(t)$ value, $f_{Lu/Hf}$, single-stage model age ($T_{DM1}$) and two-stage model age ($T_{DM2}$) are defined as in Zheng et al (2007).

# 4 Results

The zircon LA ICP-MS U-Pb data of these samples are given in Table 2, major and trace element compositions in Table 3, whole-rock Sr-Nd isotopic data in Table 4, and zircon Hf isotopic data in Table 5.

## 4.1 Zircon U–Pb data

Zircon grains from syenites (samples DMJ13) are generally euhedral to subhedral, have lengths of 120–300 mm, and have length-to-width ratios of 2:1 to 3:1 (Fig. 3a). The majority of these zircons are colorless or light brown, prismatic, and transparent to translucent, and have weak oscillatory zoning visible during cathodoluminescence (CL) imaging. The 12 spot analyses of zircons from sample DMJ13 yielded high Th (199–1306 ppm) and U (206–1893 ppm) concentrations with Th/U ratios of 0.58–1.34 that are indicative of a magmatic origin (Hoskin and Schaltegger, 2003). These spots yield $^{206}Pb/^{238}U$ ages ranging from 113.0±1.0 to 117±1.0 Ma, with a weighted mean age of 115.3±0.9 Ma (MSWD=0.74, $n$=12, 1σ; Fig. 4a and b). Zircons from the granites (sample PM2-100) (Fig. 3b) are subhedral and partly prismatic, have weak oscillatory zoning visible under CL images. A total of 16 analyses yielded high Th (210–1318 ppm) and U (314–2388 ppm) concentrations and Th/U values of 0.38–1.44. Their analytical data yield $^{206}Pb/^{238}U$ ages ranging from 113.0±1.0 to 117±1.0 Ma, with a weighted mean age of 115.7±0.8 Ma (MSWD=1.5,

**Table 2 Results of zircon LA-ICP-MS U-Pb data for the syenite and granite in the Tengchong block**

| analysis | content (ppm) | | ratios | | | | | | | | | ages(Ma) | | | | | | | |
|---|---|---|---|---|---|---|---|---|---|---|---|---|---|---|---|---|---|---|---|
| | Th | U | Th/U | $^{207}Pb/^{206}Pb$ | 1σ | $^{207}Pb/^{235}U$ | 1σ | $^{206}Pb/^{238}U$ | 1σ | $^{208}Pb/^{232}Th$ | 1σ | $^{207}Pb/^{206}Pb$ | 1σ | $^{207}Pb/^{235}U$ | 1σ | $^{206}Pb/^{238}U$ | 1σ | $^{208}Pb/^{232}Th$ | 1σ |
| Location1 DML13 syenite (N: 25°16.056′ E: 98°35.525′) | | | | | | | | | | | | | | | | | | | |
| spot-1 | 581 | 843 | 0.69 | 0.04924 | 0.00235 | 0.12115 | 0.00564 | 0.01784 | 0.00018 | 0.00564 | 0.00005 | 159 | 110 | 116 | 5 | 114 | 1 | 114 | 1 |
| spot-2 | 1306 | 976 | 1.34 | 0.04995 | 0.0021 | 0.126 | 0.00516 | 0.0183 | 0.00018 | 0.00578 | 0.00004 | 193 | 99 | 120 | 5 | 117 | 1 | 116.4 | 0.8 |
| spot-3 | 492 | 718 | 0.69 | 0.05078 | 0.00121 | 0.12582 | 0.0018 | 0.01797 | 0.00016 | 0.00546 | 0.00005 | 231 | 17 | 120 | 2 | 115 | 1 | 110 | 1 |
| spot-4 | 467 | 468 | 1.00 | 0.04891 | 0.00203 | 0.12399 | 0.005 | 0.01839 | 0.00018 | 0.00582 | 0.00004 | 144 | 96 | 119 | 5 | 117 | 1 | 117.3 | 0.8 |
| spot-5 | 199 | 211 | 0.94 | 0.04722 | 0.00409 | 0.11661 | 0.01003 | 0.01791 | 0.0002 | 0.00569 | 0.00012 | 60 | 192 | 112 | 9 | 114 | 1 | 115 | 2 |
| spot-6 | 436 | 748 | 0.58 | 0.05215 | 0.0015 | 0.13182 | 0.0036 | 0.01833 | 0.00017 | 0.00576 | 0.00004 | 292 | 67 | 126 | 3 | 117 | 1 | 116 | 0.9 |
| spot-7 | 606 | 811 | 0.75 | 0.05139 | 0.00169 | 0.12696 | 0.004 | 0.01792 | 0.00017 | 0.00564 | 0.00004 | 258 | 77 | 121 | 4 | 114 | 1 | 113.6 | 0.9 |
| spot-8 | 781 | 1125 | 0.69 | 0.05203 | 0.00172 | 0.12997 | 0.00412 | 0.01812 | 0.00017 | 0.00569 | 0.00004 | 287 | 77 | 124 | 4 | 116 | 1 | 114.7 | 0.9 |
| spot-9 | 718 | 1117 | 0.64 | 0.04995 | 0.00144 | 0.12201 | 0.00331 | 0.01772 | 0.00017 | 0.00559 | 0.00004 | 193 | 68 | 117 | 3 | 113 | 1 | 112.7 | 0.9 |
| spot-10 | 237 | 206 | 1.15 | 0.05003 | 0.00166 | 0.12533 | 0.00338 | 0.01817 | 0.00018 | 0.00548 | 0.00006 | 196 | 44 | 120 | 3 | 116 | 1 | 110 | 1 |
| spot-11 | 1265 | 1893 | 0.67 | 0.05045 | 0.00111 | 0.12477 | 0.00145 | 0.01794 | 0.00016 | 0.00544 | 0.00004 | 216 | 13 | 119 | 1 | 115 | 1 | 109.7 | 0.8 |
| spot-12 | 341 | 460 | 0.74 | 0.04605 | 0.00491 | 0.11522 | 0.01222 | 0.01815 | 0.0002 | 0.00596 | 0.0003 | | 215 | 111 | 11 | 116 | 1 | 120 | 6 |
| Location 2 PM2-100 granite (N: 25°57.738′E: 98°42.948′) | | | | | | | | | | | | | | | | | | | |
| spot-1 | 475 | 584 | 0.81 | 0.04966 | 0.00121 | 0.12534 | 0.00196 | 0.01831 | 0.00016 | 0.00558 | 0.00005 | 179 | 21 | 120 | 2 | 117 | 1 | 112 | 1 |
| spot-2 | 377 | 673 | 0.56 | 0.05054 | 0.00121 | 0.12715 | 0.0019 | 0.01824 | 0.00016 | 0.00569 | 0.00006 | 220 | 19 | 122 | 2 | 117 | 1 | 115 | 1 |
| spot-3 | 210 | 405 | 0.52 | 0.05001 | 0.00169 | 0.12524 | 0.00405 | 0.01817 | 0.00017 | 0.00573 | 0.00004 | 195 | 80 | 120 | 4 | 116 | 1 | 115.6 | 0.9 |
| spot-4 | 578 | 844 | 0.69 | 0.04979 | 0.00118 | 0.12195 | 0.00177 | 0.01776 | 0.00016 | 0.00542 | 0.00005 | 185 | 18 | 117 | 2 | 113 | 1 | 109 | 1 |
| spot-5 | 734 | 630 | 1.17 | 0.05067 | 0.00124 | 0.12749 | 0.00199 | 0.01825 | 0.00016 | 0.0055 | 0.00005 | 226 | 20 | 122 | 2 | 117 | 1 | 111 | 1 |
| spot-6 | 1318 | 2388 | 0.55 | 0.04846 | 0.00128 | 0.11957 | 0.00295 | 0.0179 | 0.00017 | 0.00567 | 0.00004 | 122 | 63 | 115 | 3 | 114 | 1 | 114.3 | 0.9 |
| spot-7 | 666 | 821 | 0.81 | 0.05102 | 0.00279 | 0.126 | 0.00676 | 0.01791 | 0.0002 | 0.00564 | 0.00004 | 242 | 128 | 120 | 6 | 114 | 1 | 113.7 | 0.8 |
| spot-8 | 758 | 690 | 1.10 | 0.05197 | 0.00124 | 0.12891 | 0.0019 | 0.01799 | 0.00016 | 0.00557 | 0.00005 | 284 | 18 | 123 | 2 | 115 | 1 | 112 | 1 |
| spot-9 | 212 | 361 | 0.59 | 0.05285 | 0.00144 | 0.1324 | 0.00258 | 0.01817 | 0.00017 | 0.00536 | 0.00005 | 322 | 27 | 126 | 2 | 116 | 1 | 108 | 1 |
| spot-10 | 367 | 668 | 0.55 | 0.05109 | 0.00125 | 0.1283 | 0.00199 | 0.01821 | 0.00016 | 0.00564 | 0.00005 | 245 | 20 | 123 | 2 | 116 | 1 | 114 | 1 |
| spot-11 | 498 | 977 | 0.51 | 0.04804 | 0.00135 | 0.12113 | 0.00248 | 0.01829 | 0.00017 | 0.00564 | 0.00007 | 101 | 31 | 116 | 2 | 117 | 1 | 114 | 1 |
| spot-12 | 275 | 715 | 0.38 | 0.05026 | 0.00128 | 0.1268 | 0.00216 | 0.0183 | 0.00017 | 0.00565 | 0.00006 | 207 | 23 | 121 | 2 | 117 | 1 | 114 | 1 |
| spot-13 | 729 | 861 | 0.85 | 0.05247 | 0.00125 | 0.13237 | 0.00188 | 0.0183 | 0.00016 | 0.00574 | 0.00005 | 306 | 17 | 126 | 2 | 117 | 1 | 116 | 1 |
| spot-14 | 403 | 314 | 1.28 | 0.0483 | 0.00115 | 0.12136 | 0.00173 | 0.01822 | 0.00016 | 0.00567 | 0.00005 | 114 | 18 | 116 | 2 | 116 | 1 | 114 | 1 |
| spot-15 | 545 | 378 | 1.44 | 0.04977 | 0.0013 | 0.12169 | 0.00214 | 0.01773 | 0.00016 | 0.00585 | 0.00008 | 184 | 24 | 117 | 2 | 113 | 1 | 118 | 2 |
| spot-16 | 755 | 970 | 0.78 | 0.04751 | 0.00118 | 0.11843 | 0.00185 | 0.01808 | 0.00016 | 0.00568 | 0.00005 | 75 | 21 | 114 | 2 | 116 | 1 | 114 | 1 |

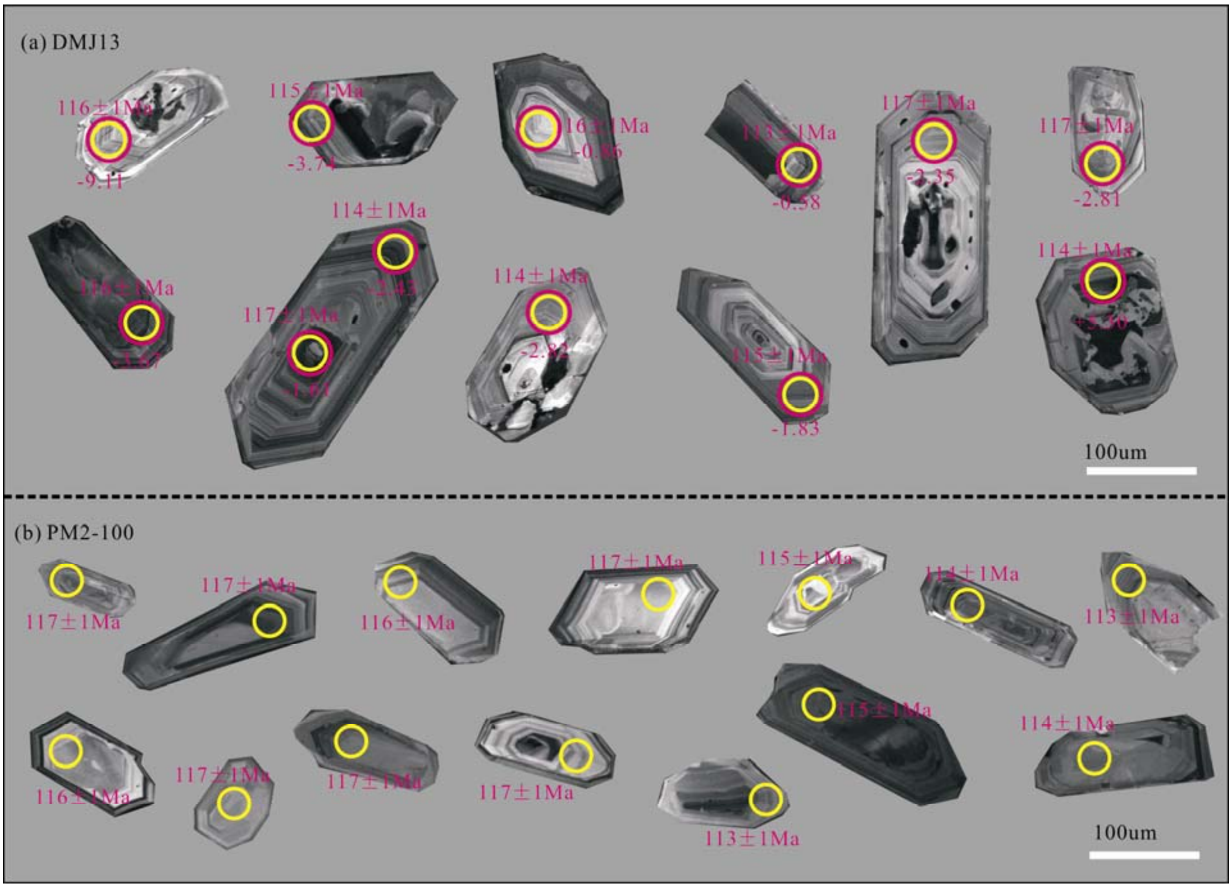


Fig. 3. Zircon CL images of representative zircon grains for the syenites and granites in the Tengchong block, SW China.

*n*=16, 1σ; Fig. 4c and d).

**4.2 Whole-rock geochemistry**

The samples from northern part of Menglian batholith are peralkaline and ferroan, belongs to the syenite (Fig. 5a–d). The samples from Gaoligong belt in the northeastern Tengchong block are high-K calc-alkali (no shown in the $SiO_2$ vs. $K_2O$ diagram) and metaluminous to peraluminous, belong to the granite (Fig. 5a–d). Both of them are similar to the early Cretaceous rocks in the Tengchong block and early Cretaceous granitoids from Gaoligong belt (Fig. 5a–d).

The syenite have low $SiO_2$=62.01–63.02 wt%, notably high $Na_2O$ (7.04–7.24 wt% with $Na_2O/K_2O$=2.02–2.10) and $Na_2O+K_2O$=10.5–10.7 (Fig. 5a). They display moderate $Al_2O_3$ concentrations of 15.17–15.36 wt% with A/CNK (molar $Al_2O_3/CaO+Na_2O+K_2O$) values of 0.74 (Fig. 5b). The primitive-mantle-normalized multi-element variation diagrams (Fig. 6a) are characterized by positive large-ion lithophile element (LILE; e.g., Rb, Th, U, K, and Pb) anomalies and obvious negative high field strength element (HFSE; e.g. Nb, Ta, P, and Ti) anomalies. These samples show high total REE concentrations of 241.5–259.9 ppm and enrichment in light REEs (LREEs) (Fig. 6b) with relative high $(La/Yb)_N$ values of 20.7–21.3, and clearly negative Eu anomalies (dEu = 0.53–0.56), suggesting insignificant fractionation of plagioclase.

The granites have high $SiO_2$ content (71.35–74.47 wt%), relative moderate $K_2O$=2.79–3.68 wt% with various $K_2O/Na_2O$ ratios=0.82–1.17, and moderate $Al_2O_3$=12.34–14.93 wt% with A/CNK=0.91–1.07, which belong to the metaluminous to peraluminous (Fig. 5b). They also show lower $Fe_2O_3T$, $TiO_2$, and MgO content than the syenites. The primitive-mantle-normalized multi-element variation diagrams (Fig. 6a) are also characterized by positive large-ion lithophile element (LILE; e.g., Rb, Th, U, K, and Pb) anomalies and more obvious negative high field strength element (HFSE; e.g. Nb, Ta, P, and Ti) anomalies than syenite. These samples show low total REE concentrations of 107.3–148.5 ppm and more enrichment in light REEs (LREEs) (Fig. 6b) with notably high $(La/Yb)_N$ values of 23.1–29.1, but clearly unsignificant Eu anomalies (*d*Eu=0.98–1.10), implying negligible fractional of plagioclase.

**4.3 Whole-rock Sr–Nd isotopes**

Whole-rock Sr–Nd isotopic data for the syenite and granite from the Tengchong block are listed in Table 4. All

**Table 3 Major (wt%) and trace element (ppm) data for the syenite-granite in the Tengchong block**

| Sample | Syenite | | | Granite | | |
|---|---|---|---|---|---|---|
| | DMJ-08 | DMJ-12 | DMJ-13 | PM2-103 | PM2-104 | PM2-105 |
| $SiO_2$ | 63.03 | 62.01 | 62.92 | 74.41 | 71.35 | 72.40 |
| $TiO_2$ | 0.47 | 0.51 | 0.48 | 0.32 | 0.30 | 0.30 |
| $Al_2O_3$ | 15.20 | 15.36 | 15.17 | 12.34 | 14.93 | 14.20 |
| MgO | 0.74 | 0.85 | 0.78 | 0.54 | 0.64 | 0.60 |
| $Fe_2O_3T$ | 3.64 | 4.31 | 4.09 | 2.32 | 2.24 | 2.29 |
| CaO | 2.82 | 2.83 | 2.88 | 2.74 | 2.70 | 2.56 |
| $Na_2O$ | 7.11 | 7.24 | 7.04 | 3.42 | 3.36 | 3.15 |
| $K_2O$ | 3.47 | 3.44 | 3.49 | 2.79 | 3.27 | 3.68 |
| MnO | 0.06 | 0.06 | 0.06 | 0.04 | 0.04 | 0.04 |
| $P_2O_5$ | 0.14 | 0.16 | 0.15 | 0.11 | 0.11 | 0.11 |
| LOI | 3.12 | 3.12 | 3.28 | 0.94 | 0.71 | 0.91 |
| total | 99.80 | 99.89 | 100.33 | 99.98 | 99.65 | 100.24 |
| Li | 9.01 | 11.3 | 10.3 | 27.1 | 22.8 | 25.1 |
| Be | 2.74 | 2.93 | 2.86 | 1.72 | 1.71 | 1.49 |
| Sc | 18.5 | 19.4 | 18.0 | 9.6 | 10.6 | 9.4 |
| V | 28.7 | 33.8 | 30.9 | 33.5 | 29.5 | 30.7 |
| Cr | 5.71 | 6.51 | 17.4 | 9.31 | 7.52 | 5.68 |
| Co | 14.5 | 9.99 | 10.1 | 50.4 | 47.1 | 44.5 |
| Ni | 2.58 | 3.08 | 8.33 | 8.09 | 4.82 | 4.43 |
| Cu | 3.9 | 3.9 | 4.29 | 3.72 | 3.75 | 3.36 |
| Zn | 83.8 | 84 | 85 | 98 | 49.3 | 62.9 |
| Ga | 17.7 | 18.1 | 17.8 | 15.5 | 15.7 | 14.4 |
| Ge | 1.19 | 1.22 | 1.2 | 0.96 | 0.97 | 0.93 |
| As | 1.43 | 1.34 | 1.4 | 1.66 | 0.89 | 1.31 |
| Rb | 99.3 | 93.4 | 96.6 | 103 | 122 | 129 |
| Sr | 440 | 439 | 446 | 269 | 287 | 287 |
| Y | 23.6 | 23.6 | 23.5 | 9.3 | 9.93 | 8.13 |
| Zr | 222 | 238 | 216 | 194 | 181 | 176 |
| Nb | 16.5 | 15.8 | 15.6 | 9.05 | 8.75 | 8 |
| Mo | 0.09 | 0.16 | 0.35 | 0.64 | 0.26 | 1.45 |
| Cs | 1.51 | 1.64 | 1.55 | 5.74 | 5.69 | 5.61 |
| Ba | 539 | 510 | 531 | 614 | 636 | 796 |
| La | 59.5 | 63.4 | 59.7 | 29 | 35.1 | 32.1 |
| Ce | 112 | 118 | 108 | 50.5 | 61.5 | 56.4 |
| Pr | 12 | 13 | 12 | 4.71 | 5.54 | 5.05 |
| Nd | 38.1 | 41.9 | 39.1 | 14.4 | 16.8 | 15 |
| Sm | 6.08 | 6.7 | 6.16 | 2.14 | 2.4 | 2.28 |
| Eu | 1.05 | 1.07 | 1.02 | 0.73 | 0.70 | 0.71 |
| Gd | 5.46 | 5.62 | 5.31 | 1.90 | 2.02 | 1.67 |
| Tb | 0.72 | 0.73 | 0.72 | 0.25 | 0.28 | 0.24 |
| Dy | 3.88 | 3.81 | 3.75 | 1.41 | 1.57 | 1.23 |
| Ho | 0.75 | 0.71 | 0.75 | 0.29 | 0.31 | 0.25 |
| Er | 2.29 | 2.18 | 2.26 | 0.84 | 0.94 | 0.75 |
| Tm | 0.32 | 0.32 | 0.33 | 0.12 | 0.14 | 0.11 |
| Yb | 2.04 | 2.14 | 2.07 | 0.9 | 1.02 | 0.79 |
| Lu | 0.31 | 0.33 | 0.32 | 0.14 | 0.16 | 0.13 |
| Hf | 4.89 | 5.76 | 5.25 | 4.15 | 4.17 | 3.82 |
| Ta | 1.49 | 1.36 | 1.4 | 0.84 | 1.08 | 0.78 |
| W | 60.3 | 34.5 | 36.8 | 270 | 303 | 269 |
| Tl | 0.46 | 0.48 | 0.48 | 0.55 | 0.5 | 0.48 |
| Pb | 28.6 | 27.9 | 25.4 | 24.9 | 25.2 | 24.9 |
| Bi | 0.057 | 0.052 | 0.046 | 0.04 | 0.049 | 0.007 |
| Th | 35.64 | 36.72 | 31.93 | 16.91 | 18.58 | 15.98 |
| U | 4.51 | 4.29 | 3.92 | 3.10 | 3.63 | 2.23 |
| $Mg^{\#}$ | 32.11 | 31.43 | 30.78 | 35.37 | 39.83 | 37.78 |
| A/CNK | 0.74 | 0.74 | 0.74 | 0.91 | 1.07 | 1.03 |
| ΣREE | 244.50 | 259.90 | 241.49 | 107.33 | 128.48 | 116.71 |

the initial $^{87}Sr/^{86}Sr$ isotopic ratios ($I_{Sr}$) and $\varepsilon Nd(t)$ values are calculated according to the LA-ICP-MS zircon U-Pb dates for the syenite and granite.

The syenite (samples DMJ13) are relative high Sr content=439 ppm and moderate Rb content=93.4 ppm, and which have initial $^{87}Sr/^{86}Sr$=0.713013, high $^{143}Nd/^{144}Nd$ ratios=0.512121 with $\varepsilon Nd(t)$ values of −6.8, and two-stage Nd model ages of 1.26Ga. The granites (sample PM2-105 and PM2-105-1) share similar Sr and Rb contents including relative low Sr=287 ppm and Rb=129 ppm. They have lower intial $^{87}Sr/^{86}Sr$ (0.703408 and 0.704241) and $^{143}Nd/^{144}Nd$ ratio (0.512051 and 0.512067) with $\varepsilon Nd(t)$ values of −3.8 and −3.5, and two-stage Nd model ages of 1.33–1.35Ga.

As shown in the $\varepsilon Nd(t)$ vs. initial $^{87}Sr/^{86}Sr$ diagram, the granite samples share the similar characters with the granitoids and volcanic rocks from TransHimalaya batholith and the syenite are similar to the granitoids and volcanic rocks among the Tengchong and central and northern Lhasa blocks and TransHimalaya batholith (Fig. 6a) (Yang et al., 2006; Zhu et al., 2009; Qu et al., 2012; Lin et al., 2012; Chen et al., 2014; Zhu et al., 2015b). Both of them are plotted into the evolutionary line between the arc-setting basalts and lower- and upper-crust (Fig. 7).

### 4.4 Zircon chemical and Lu-Hf isotopic compositions

The zircons from dated samples were also analyzed for Lu-Hf isotopes on the same domains, and the results are listed in Table 5. Initial $^{176}Hf/^{177}Hf$ ratios and $\varepsilon Hf(t)$ values of the zircons were calculated according to their LA-ICP-MS zircon U-Pb dates for the syenite. We selected 12 zircon grains from the syenite (DMJ13) for Lu-Hf isotopic analysis. All of these spots display concordant zircon U-Pb dating, which have various and relative enriched Hf isotopic compositions with $\varepsilon Hf(t)$ values ranging from −9.11 to −0.27(but one is +5.30), with corresponding two-stage Hf model ages of 1.18 to 1.75Ga(but one is 0.83Ga). Above these various Hf compositions possibly indicate the more ancient continental crust (Yang et al., 2007; Zheng et al., 2007).

Furthermore, zircons from both syenite and moznogranite have moderate Th and U content and most of their Th/U ratios are distributed in the near the line of

**Table 4 Whole-rock Sr-Nd isotopic data for the syenite and granite in the Tengchong block**

| Sample | $^{87}Sr/^{86}Sr$ | 2 sm | Sr (ppm) | Rb (ppm) | $^{143}Nd/^{144}Nd$ | 2 sm | Nd (ppm) | Sm (ppm) | $T_{2DM}$ (Ga) | $\varepsilon Nd(t)$ | $(^{87}Sr/^{86}Sr)i$ | $(^{143}Nd/^{144}Nd)i$ |
|---|---|---|---|---|---|---|---|---|---|---|---|---|
| DMJ-12 | 0.714011 | 0.000011 | 439 | 93.4 | 0.512213 | 0.000007 | 41.9 | 6.7 | 1.26 | −6.83 | 0.713013 | 0.512141 |
| PM2-105 | 0.712916 | 0.000015 | 287 | 129 | 0.512122 | 0.000012 | 15 | 2.28 | 1.35 | −3.80 | 0.704241 | 0.512051 |
| PM2-105-1 | 0.712082 | 0.000008 | 287 | 129 | 0.512138 | 0.000004 | 15 | 2.28 | 1.33 | −3.48 | 0.703408 | 0.512067 |

$^{87}Rb/^{86}Sr$ and $^{147}Sm/^{144}Nd$ ratios were calculated using Rb, Sr, Sm and Nd contents analyzed by ICP-MS.

$T_{2DM}$ represent the two-stage model age and were calculated using present-day $(^{147}Sm/^{144}Nd)_{DM}$=0.2137, $(^{147}Sm/^{144}Nd)_{DM}$=0.51315 and $(^{147}Sm/^{144}Nd)crust$=0.1012. $\varepsilon Nd(t)$ values were calculated using present-day $(^{147}Sm/^{144}Nd)_{CHUR}$=0.1967 and $(^{147}Sm/^{144}Nd)_{CHUR}$=0.512638.

$\varepsilon Nd(t)=[(^{143}Nd/^{144}Nd)\ sample(t)/(^{143}Nd/^{144}Nd)CHUR(t)\ -1]\times104$, $T_{2DM}=1/\lambda\times\{1+[(^{143}Nd/^{144}Nd)sample-((^{147}Sm/^{144}Nd)sample-(^{147}Sm/^{144}Nd)crust)\times(e^{\lambda t}-1)-(^{143}Nd/^{144}Nd)_{DM}]/((^{147}Sm/^{144}Nd)_{crust}-(^{147}Sm/^{144}Nd)_{DM})\}$

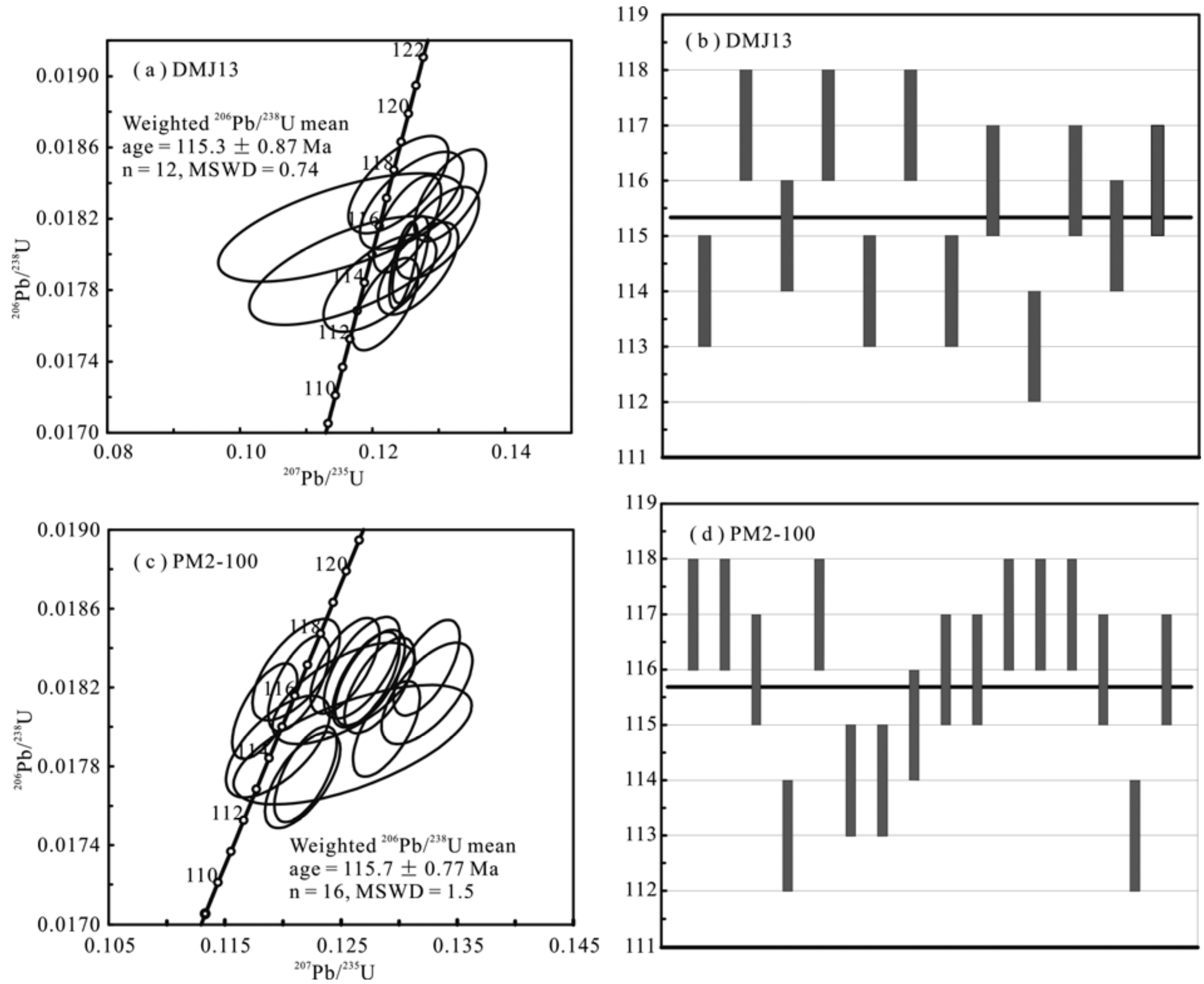


Fig. 4. LA-ICP-MS U–Pb zircon concordia diagram of representative zircon grains for the syenites and granites in the Tengchong block, SW China.

**Table 5 Single-grain zircon Hf isotopic data for the syenite and granite in the Tengchong block**

| Grain spot | Age (Ma) | $^{176}Yb/^{177}Hf$ | 2se | $^{176}Lu/^{177}Hf$ | 2se | $^{176}Hf/^{177}Hf$ | 2se | $(^{176}Hf/^{177}Hf)_i$ | $f_{Lu/Hf}$ | $\varepsilon Hf(t)$ | 2se | $T_{DM1}$ (Ma) | $T_{DMC}$ (Ma) |
|---|---|---|---|---|---|---|---|---|---|---|---|---|---|
| syenite | | | | | | | | | | | | | |
| DMJ13-01 | 111 | 0.029875 | 0.000215 | 0.000887 | 0.000006 | 0.282502 | 0.000032 | 0.282501 | −0.97 | −7.17 | 1.15 | 1058 | 1623 |
| DMJ13-02 | 114 | 0.092500 | 0.001004 | 0.002974 | 0.000032 | 0.282857 | 0.000021 | 0.282851 | −0.91 | 5.30 | 0.76 | 591 | 833 |
| DMJ13-03 | 117 | 0.064597 | 0.000324 | 0.002154 | 0.000012 | 0.282625 | 0.000050 | 0.282620 | −0.94 | −2.81 | 1.76 | 917 | 1351 |
| DMJ13-04 | 119 | 0.072887 | 0.000643 | 0.002387 | 0.000023 | 0.282657 | 0.000031 | 0.282652 | −0.93 | −1.65 | 1.11 | 876 | 1279 |
| DMJ13-05 | 115 | 0.057979 | 0.000287 | 0.001607 | 0.000009 | 0.282653 | 0.000013 | 0.282649 | −0.95 | −1.83 | 0.45 | 864 | 1287 |
| DMJ13-06 | 111 | 0.048472 | 0.000208 | 0.001799 | 0.000017 | 0.282699 | 0.000025 | 0.282695 | −0.95 | −0.27 | 0.88 | 801 | 1185 |
| DMJ13-07 | 110 | 0.057137 | 0.000235 | 0.001723 | 0.000019 | 0.282642 | 0.000016 | 0.282638 | −0.95 | −2.32 | 0.56 | 882 | 1315 |
| DMJ13-08 | 117 | 0.047868 | 0.000160 | 0.001316 | 0.000005 | 0.282636 | 0.000017 | 0.282633 | −0.96 | −2.35 | 0.60 | 881 | 1322 |
| DMJ13-09 | 114 | 0.048990 | 0.000289 | 0.001611 | 0.000007 | 0.282625 | 0.000028 | 0.282621 | −0.95 | −2.82 | 1.00 | 903 | 1350 |
| DMJ13-10 | 107 | 0.039665 | 0.000382 | 0.001372 | 0.000009 | 0.282655 | 0.000053 | 0.282652 | −0.96 | −1.90 | 1.88 | 855 | 1286 |
| DMJ13-11 | 104 | 0.049328 | 0.000362 | 0.001746 | 0.000013 | 0.282584 | 0.000040 | 0.282581 | −0.95 | −4.47 | 1.43 | 965 | 1447 |
| DMJ13-12 | 117 | 0.040564 | 0.000242 | 0.001165 | 0.000005 | 0.282657 | 0.000017 | 0.282654 | −0.96 | −1.61 | 0.59 | 848 | 1275 |
| DMJ13-13 | 114 | 0.047802 | 0.000174 | 0.001352 | 0.000005 | 0.282636 | 0.000014 | 0.282633 | −0.96 | −2.43 | 0.48 | 882 | 1325 |
| DMJ13-14 | 116 | 0.072374 | 0.000232 | 0.002424 | 0.000010 | 0.282602 | 0.000027 | 0.282596 | −0.93 | −3.67 | 0.97 | 958 | 1405 |
| DMJ13-15 | 113 | 0.056633 | 0.000182 | 0.001582 | 0.000004 | 0.282689 | 0.000016 | 0.282686 | −0.95 | −0.58 | 0.58 | 811 | 1206 |
| DMJ13-16 | 110 | 0.048512 | 0.000295 | 0.001349 | 0.000009 | 0.282680 | 0.000013 | 0.282678 | −0.96 | −0.93 | 0.46 | 818 | 1226 |
| DMJ13-17 | 116 | 0.062370 | 0.000072 | 0.002177 | 0.000004 | 0.282680 | 0.000025 | 0.282676 | −0.93 | −0.86 | 0.87 | 836 | 1227 |
| DMJ13-18 | 115 | 0.062080 | 0.000740 | 0.001864 | 0.000039 | 0.282599 | 0.000016 | 0.282595 | −0.94 | −3.74 | 0.57 | 947 | 1409 |
| DMJ13-19 | 116 | 0.048355 | 0.000044 | 0.001691 | 0.000002 | 0.282446 | 0.000039 | 0.282443 | −0.95 | −9.11 | 1.38 | 1161 | 1749 |
| DMJ13-20 | 120 | 0.079978 | 0.000341 | 0.002598 | 0.000011 | 0.282686 | 0.000023 | 0.282680 | −0.92 | −0.62 | 0.82 | 838 | 1214 |

Th/U ratio=1.0, which plotted in the field of the zircon in the Lhasa Terrane records of continental crustal reworking during Mesozoic-Cenozoic magmatisms (Liu et al., 2014) (Fig. 8). They also display the high U/Yb ratios and moderate Y content , suggesting the typical continental crust characters rather than the recycled oceanic crust

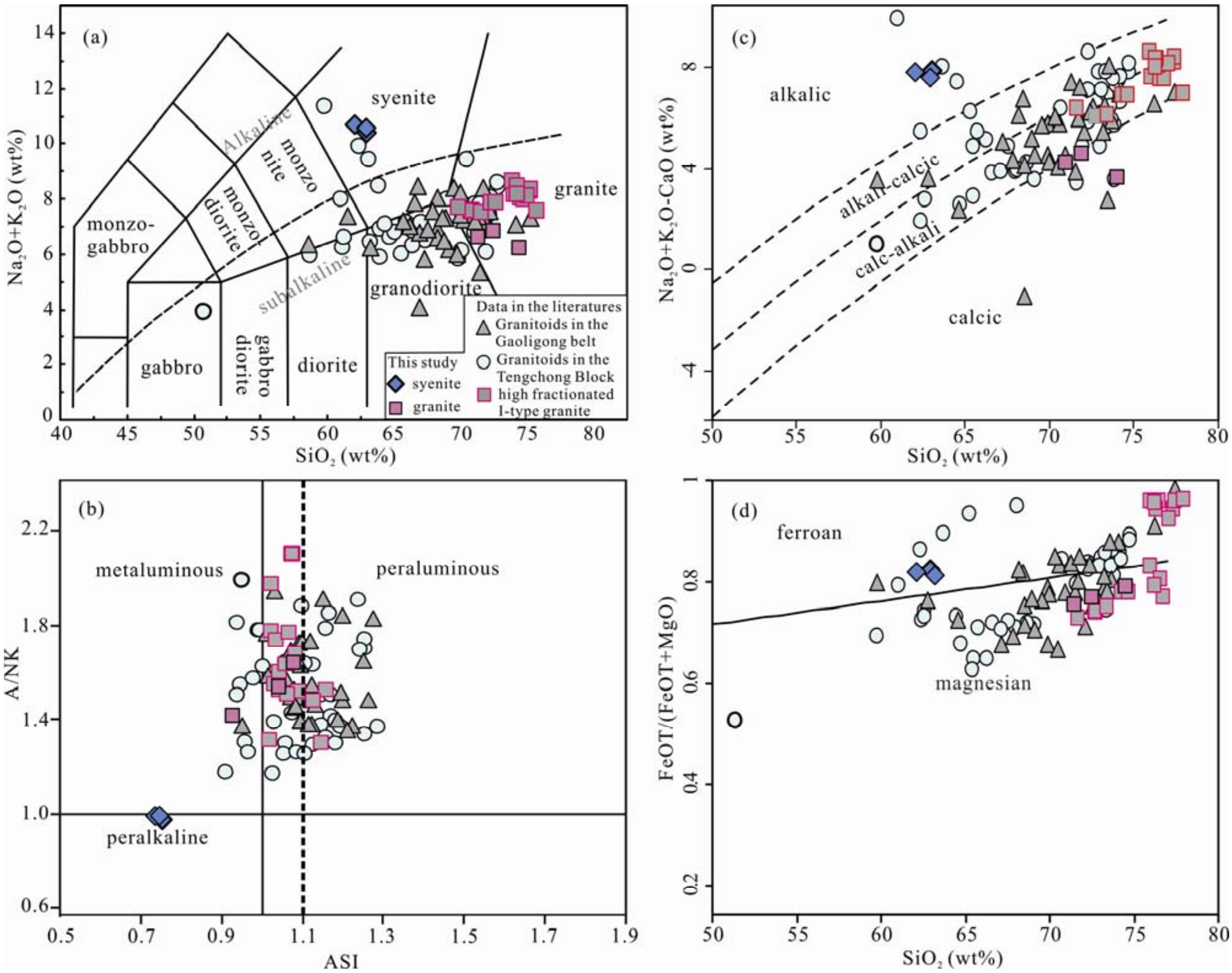


Fig. 5. (a), ($Na_2O+K_2O$) vs $SiO_2$ diagram; (b), A/NK vs. A/CNK diagram; (c), ($Na_2O+K_2O$–CaO) vs $SiO_2$ diagram; (d), FeOT/(FeOT/MgO) vs. $SiO_2$ diagram.

All of them are referenced by Frost et al. (2001). The data of early Cretaceous granitoids in the Gaoligong belt from Yang et al. (2006); The data of early Cretaceous granitoids in the Tengchong block from Cong et al. (2011a, b), Qi et al. (2011), Li et al. (2012), Luo et al. (2012), and (Cao et al. 2014); The data of high fractionated I-type granites in the Tengchong block from Zhu et al. (2015).

(Grimes et al., 2007) (Fig. 8).

## 5 Discussion

### 5.1 Petrogenesis of the syenite

Yang et al. (2012) has summarized several models to interpret the genesis of the syenite: extensive differentiation from mantle-derived basaltic magmas (Litvinovsky et al., 2002; Yang et al., 2005), magma mixing between basic and silicic melts with subsequent differentiation of the hybrid melts/liquids(Dorais, 1990; Sheppard, 1995; Riishuus et al., 2005; Yang et al., 2008), and partial melting of crustal rocks at high pressures (Huang and Wyllie, 1975; Lubala et al., 1994; Yang et al., 2012). Before any further discussions, it is important to distinguish the silica-saturated and silica-undersaturated syenites, as we will know whether it was derived from normal magmatic series or special alkaline series or not. The presence of the quartz can be up to 5–10% and absence of nepheline-bearing in the syenites may infer that the Early Cretaceous syenites belong to the silica-saturated syenites (Fig. 2a and b), similar with the silica-saturated syenites in northern China Craton (Yang et al., 2012). The syenites have been characterized by low abundances of MgO=0.74–0.85 wt%, $Fe_2O_3T$=3.64–4.31 wt%, $TiO_2$= 0.47–0.51 wt%, and Cr (5.71–17.4 ppm) and Ni (2.58–8.33 ppm) (Table 2), which may preclude the model of differentiation from mantle-derived basaltic magmas but indicate a product from fractionation of alkaline magmas derived from an enriched mantle and/or a continental crust source. The absence of related early Cretaceous ultramafic to mafic rocks in the Tengchong block (Y.B.G.M.R., 1991) and associated mafic magmatic enclaves in the syenites (Fig. 2a) also preclude the conclusion of magma mixing between basic and felsic melts, although some enclaves are developed in the calc-alkaline granodiorite in the

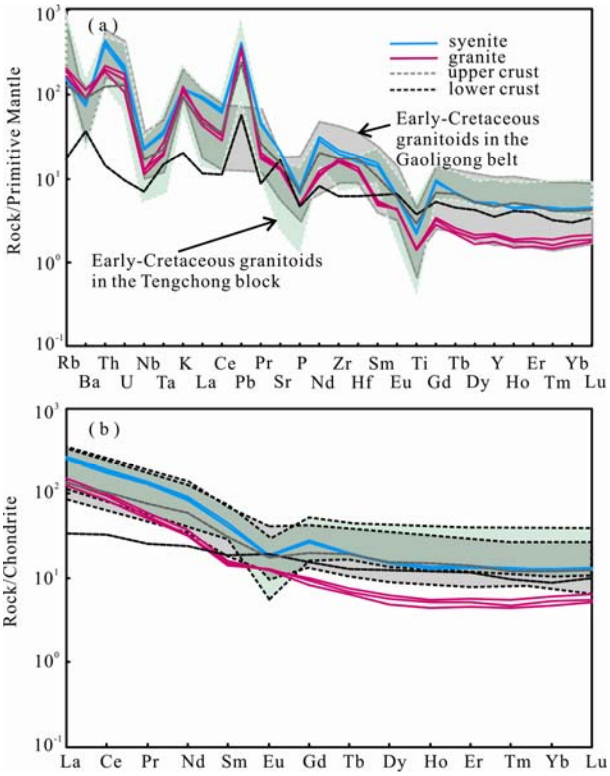


Fig. 6. Chondrite-normalized REE patterns and primitive-mantle-normalized trace element spider diagram for the syenites and granites in the Tengchong block, SW China.
The primitive mantle and chondrite values are from Sun and McDonough (1989). The data in the Tengchong Block and Gaoligong belt is same as the Fig. 5.

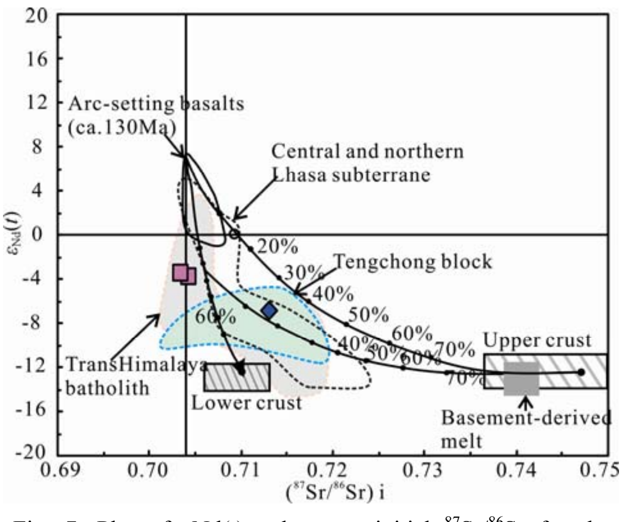


Fig. 7. Plot of $\varepsilon$Nd($t$) values vs. initial $^{87}Sr/^{86}Sr$ for the syenites and granites in the Tengchong block, SW China.
Lower continental crust (Miller et al., 1999) and upper continental crust (Harris et al., 1988). Arc-setting basalt was referenced by Chen et al. (2014). Symbols as in Fig. 5.

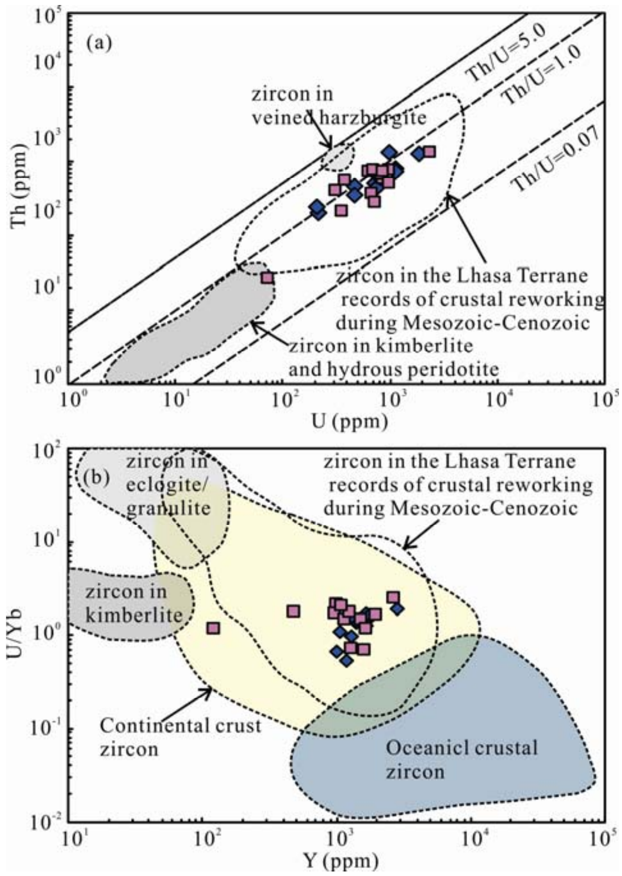


Fig. 8. Discriminant diagrams for zircon origin for the syenites and granites in the Tengchong block, SW China.
Modified from Liu et al. (2014) and Grimes et al. (2007). Symbols as in Fig. 5.

middle to southern Linaghe area which is far from our fields (Cong et al., 2011a; Li et al., 2012). The high initial $^{87}Sr/^{86}Sr$=0.713013, high $^{143}Nd/^{144}Nd$ ratios=0.512121 with $\varepsilon$Nd ($t$) values of −6.8 overlap with that of felsic granitoids in the Tengchong block and intermediate to felsic granitoids and volcanic rocks in the Central and Northern Lhasa blocks, both of which are typical continental crustal sources (Yang et al., 2006; Zhu et al., 2009; Chen et al., 2014; Zhu et al., 2015b). Then the zircon Hf components are characterized by significant negative zircon $\varepsilon$Hf($t$) values ranging from −9.11 to −0.27 (although one is positive) with two-stage Hf model ages of 1.18 to 1.75Ga (Fig. 9), which also imply the mainly Paleo - and Meso-Proterozoic continental sources (Yang et al., 2007; Zheng et al., 2007). In addition, the low Nb and Ta content and Nb/Ta ratios range from 11.1 to 11.6, which are less than those from mantle-derived melts (17.5±2.0) (Kamber and Collerson, 2000), also suggesting a crustal source. The notably high $Na_2O$ (7.04–7.24 wt%) with high $Na_2O/K_2O$ ratios=2.01–2.10 indicate a sodium-rich source.

Experimental data show that syenitic magma could be formed by the melting at the base of continental crust in two conditions (Huang and Wyllie, 1975; Johannes and Holtz, 1990): (1) partial melting of granite at Pressure>10kbar may produce the melts with low $SiO_2$ content in the water-undersaturated conditions, with the increasing normative feldspar; (2) partial melting of

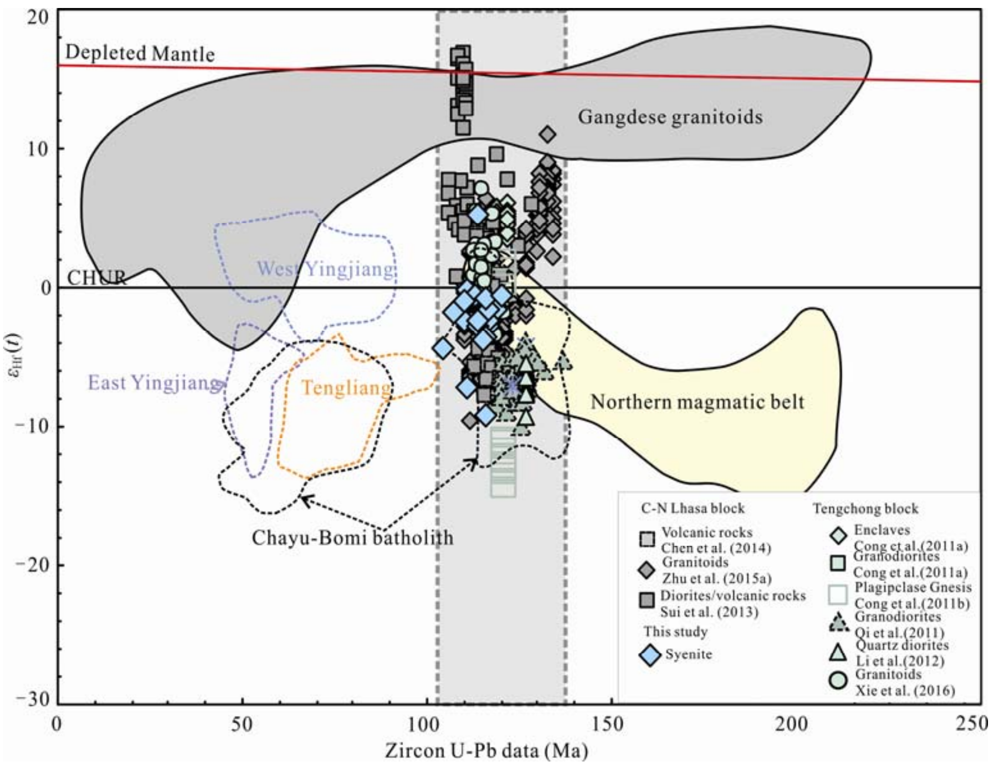


Fig. 9. Plot of zircon εHf($t$) vs. zircon U-Pb data for the syenites in the Tengchong Block, SW China.

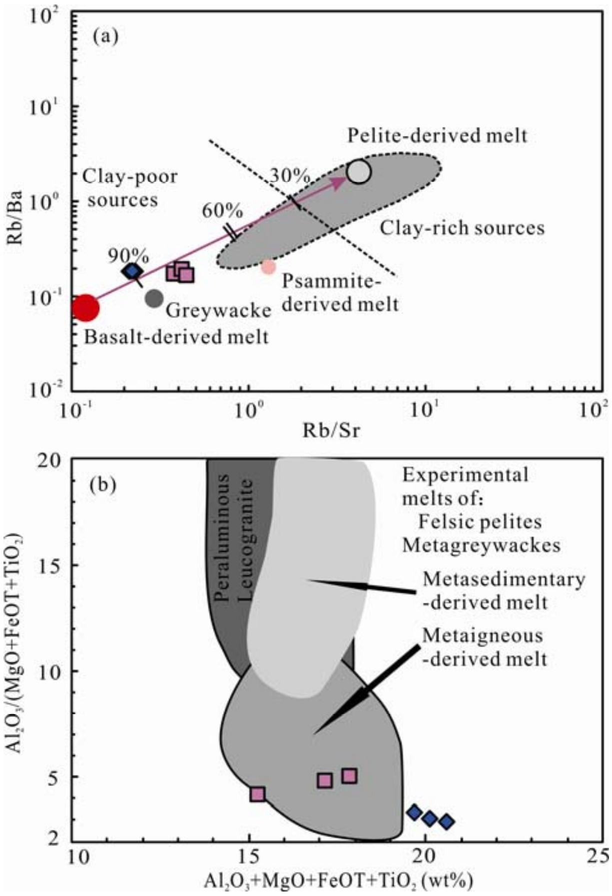


Fig. 10. Diagram of distinguishing the slab-derived and/or sediments-derived fluids/melts (modified from Wang et al., 2014; Zhao et al., 2016; Elliott, 2003). Symbols as in Fig. 5.

muscovite granite with 74 wt% $SiO_2$ under 15kbar pressure and ca. 5 wt% water, which can produced the syenitic melts. But these experimental data are suited to haplogranitic system which does not contain mafic components, contrast to our syenites. And the juvenile crustal rocks have a significant Mg, Fe, and Ca along with the elevated pressure that would leave a residual clinopyroxene and garnet, then the granitic melts would be produced rather than syenitic melts (Litvinosky and Steele, 2000). Also, experimental petrological studies show that Na-rich intermediate to felsic melts are formed by either (1) the differentiation of mantle-derived mafic magmas (Stern et al., 1989) or (2) the high-temperature dehydration melting of mafic lower-crustal material (Rapp and Watson, 1995). However, the Early Cretaceous syenite share similar evolved whole-rock initial $^{87}Sr/^{86}Sr$ and εNd(t) and zircon Hf compositions with the Early Cretaceous granitoids near the study area in the Tengchong block (Figs. 7 and 9) (Yang et al., 2006; Zhu et al., 2015b), indicating that their similar and/or common sources-melting of continental crustal materials, such as, mafic lower crustal and/or upper evolved crustal materials. Then the variable zircon Hf isotopic compositions also imply the mixing components (Kemp et al., 2007). The high Th and U abundances and moderate Y abundances and U/Yb ratios of the zircons (Fig. 8), as the robust mineral in the rocks, also show the continental crustal source. In addition, the low abundances of MgO, $Fe_2O_3T$, $TiO_2$, Cr, Ni and depletion of P and Ti (Fig. 6a) imply the significant fractional crystallization of ferro-magnesian minerals such as pyroxene, amphibole, biotite and Fe-Ti oxides and so on. The significant negative Eu anomalies (Fig. 6b) also indicate the fractionation of plagioclase. Generally, the accessory minerals would be controlled much of the REE variation (Yang et al., 2012), the higher total REE than granites (Fig. 6b) suggests more accumulation of mineral such as titanite, zircon, apatite and monzonite, which may be a crucial accessory mineral in the rocks. In addition, the MgO-$\varepsilon$Nd($t$), Ba/Th-La/Sm, Ba/Th-Th/Nb and Ba/La-Th/Nb diagram indicate that the sediments-derived fluids/melts play a key role in the genesis of the syenite (Fig. 10).

Based on the geochemical, whole-rock isotopic and zircon Hf isotopic data, we suggest that the Early Cretaceous syenites were possibly derived from mixing of mafic lower crustal and evolved sediments-derived materials, and the fractionation of some ferro-magnesian mineral and plagioclase may occur during the evolution of magma.

### 5.2 Petrogenesis of the granite

In general, the granites are crust-derived materials mainly including metabasaltic rocks and/or metasedimentary rocks. Our granites are high $SiO_2$ content (71.35–74.41 wt%) and A/CNK (0.91–1.07) (Fig. 5a and b), belong to the metaluminous to peraluminous (Frost et al., 2001), similar with the metasedimentary materials (Chappell and White, 1992). The low MgO, $Fe_2O_3T$, $TiO_2$, Cr and Ni indicate that they did not directly produce from differentiation of mantle-derived mafic magmas. On the primitive-mantle-normalized multi-element variation and REE diagrams (Fig. 6a), these granites show some features similar to that of upper crust with enrichment of LILEs (Rb, Th, U, K, and Pb) and depletion of HFSEs (Nb, Ta, P, and Ti), implying they were derived from crustal sources region (Harris et al., 1988), which was coupled with fractional crystallization to some extents during the evolution of magma. But the more differentiated pattern and depletion of HREE with high $(La/Yb)_N$=23.1–29.1 than the upper crust (Fig. 6b) indicates the some HREE-rich minerals as the residue (such as garnet and so on) (Qu et al., 2012). In addition, the less pronounced or slightly positive Eu anomalies (Fig. 6b) may imply the negligible fractional crystallization of plagioclase. The relative low MgO and $Mg^{\#}$ (Fig. 11b) prove that the possible melting of metasedimentary-derived greywacke. The low $Al_2O_3/(MgO+FeOT+TiO_2)$ and moderate $(Al_2O_3+MgO+FeOT+TiO_2)$ content (Fig. 11a) also infer that the significant involvement of metasedimentary-derived greywackes (Patiňo Douce et al., 1999). On the initial $^{87}Sr/^{86}Sr$ and $\varepsilon$Nd($t$) diagram (Fig. 7), the samples are plotted into the fields between the lower crust and arc-setting basalts (Miller et al., 1999; Chen et al., 2014), similar with igneous rocks in the TransHimalaya batholith (Lin et al., 2012). However, the majority are still typical continental crustal sources confirmed by the crustal-like zircon chemical characters (Fig. 8).

In summary, together with its whole-rock chemical and isotopic data and zircon chemical data, we suggest that the granites were derived from the melting of predominated metasedimentary greywackes in the ancient continental crust.

### 5.3 Tectonic implications

Zircon U–Pb data show that the peraluminous, high-K, calc-alkaline granites and alkaline syenite in the Tengchong block were formed at ca. 115.3–115.7 Ma, which is consistent with abundant Early Cretaceous granitoids (of age range from 143 to 115 Ma) in the Tengchong block (Yang et al., 2006; Cong et al., 2011a, b; Li et al., 2012; Luo et al., 2012; Qi et al., 2011; Xie et al., 2010; Xu et al., 2012; Cao et al., 2014; Zhu et al., 2015b). The Early Cretaceous magmatism in the Tengchong Block intensified from 135 to ~110 Ma and generated intrusions with negative zircon $e$Hf($t$) (Fig. 9) and whole-rock $e$Nd($t$) compositions (Fig. 7), peraluminous characteristics (A/CNK >1) (Zhu et al., 2015b), and dominantly Mesoproterozoic two-stage isotopic model ages (Yang et al., 2006; Cong et al., 2011a, b; Qi et al., 2011; Li et al., 2012; Xu et al., 2012; Zhu et al., 2015b; Xie et al., 2016). This led previous workers to suggest that the Early Cretaceous magmatism in the Tengchong block was dominated by magmas generated by the partial melting of ancient crustal material.

However, the geodynamical setting of the Early Cretaceous tectono-thermal magmatism in the Tengchong block has remained controversial due to: (1) the active continental margin is related to the eastward subduction of the Putao–Myitkyina paleo-oceanic slab as a branch of the Neo-Tethys Ocean (Cong et al., 2010a, 2011a, 2011b); (2) the southward subduction of the Bangong–Nujiang Tethyan oceanic slab occurred during the collision between the Lhasa–Tengchong and the Qiangtang–Baoshan blocks (Yang et al., 2006; Qi et al., 2011; Li et al., 2012; Luo et al., 2012; Cao et al., 2014; Zhu et al., 2015b); and (3) there is a post-collisional setting between the Lhasa and Qiangtang blocks being partly influenced by the far field of the Neo-Tethyan oceanic slab (Xu et al., 2012). In a recent study, Xie et al. (2016) pointed out the closely resemblance between the Early Cretaceous magmatism in the Tengchong Terrane and those in the

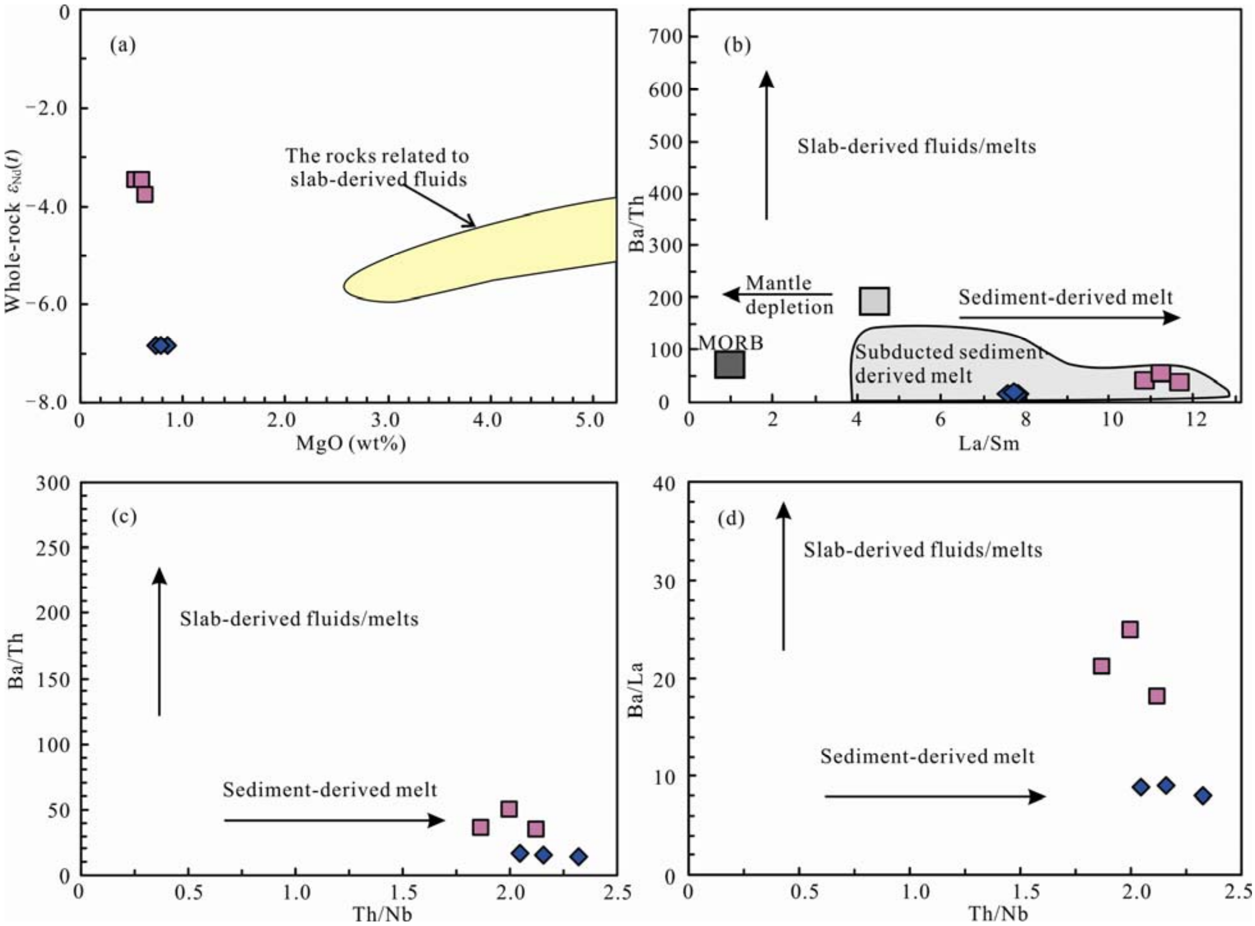


Fig. 11. (a) Rb/Ba vs Rb/Sr diagrams (Janoušek et al. 2004) and (b) compositional field of experimental melts derived from melting of felsic pelites (muscovite schists), metagreywackes and amphibolites (Patiño Douce, 1999). Symbols as in Fig. 5.

central and northern Lhasa subterranes. The geochronological, geochemical and paleomagnetic data are consistent with magma generation associated with the subduction of the Tethyan Bangong-Nujiang Ocean lithosphere (Zhu et al., 2009; 2011; 2013; 2015a; Sui et al., 2013; Chen et al., 2014; Yan et al., 2016). Investigations based on petrology, stratigraphy and paleobiogeography (YNBGMR, 1991) also suggest that the Tengchong Terrane is the eastern extension of the Lhasa Terrane (Xie et al., 2016), both of which experienced similar tectono-magmatic histories. Generally, the Early Cretaceous magmatism was regarded as the products of southward subduction of Bangong-Nujiang Meoso-Tethys (Zhu et al., 2009, 2011, 2015a; Sui et al., 2013; Chen et al., 2014; Zhu et al., 2015b; Xie et al., 2016). In recent, the slab break-off of subducting Bangong -Nujiang Tethyan oceanic lithosphere was proposed (Zhu et al., 2017b). In the slab break-off setting (Fig. 12), a hybrid basaltic magma that had affinity with arc-type and within-plate suites would be produced, the late Early Cretaceous Xainza basalts and bimodal volcanic rocks in central and northern Lhasa subterrane (Sui et al., 2013; Chen et al., 2014) (Fig. 12). Then the hybrid magma provides heat to induce partial melting of ancient lower crust, mature continental basement, and juvenile crust, which resulted in various melts (Fig. 12) including Xainza andesites and dacites (Chen et al., 2014), Daguo rhyolites (Sui et al., 2013), quartz diorite-granodiorite-monzogranite (Zhu et al., 2017b), and the granite-syenite (this study). In this study, both our whole-rock Sr-Nd isotopic and zircon Hf isotopic data share similar characteristics with the magmatism not only in the Tengchong block but also in the central and northern Lhasa subterrane (both of which were belonging to Northern Magmatic belt which mainly contained the Early-Cretaceous magmatism from central and northern Lhasa to Tengchong block (Xu et al., 1985; Zhu et al., 2011; Xu et al., 2012). Therefore, we infer that the Early Cretaceous syenites and granites are also the products that associated to the slab break-off of subducted Bangong-Nujiang Meso-Tethys oceanic lithosphere.

## 6 Conclusions

(1) Zircon LA ICP-MS U-Pb data show that the syenites

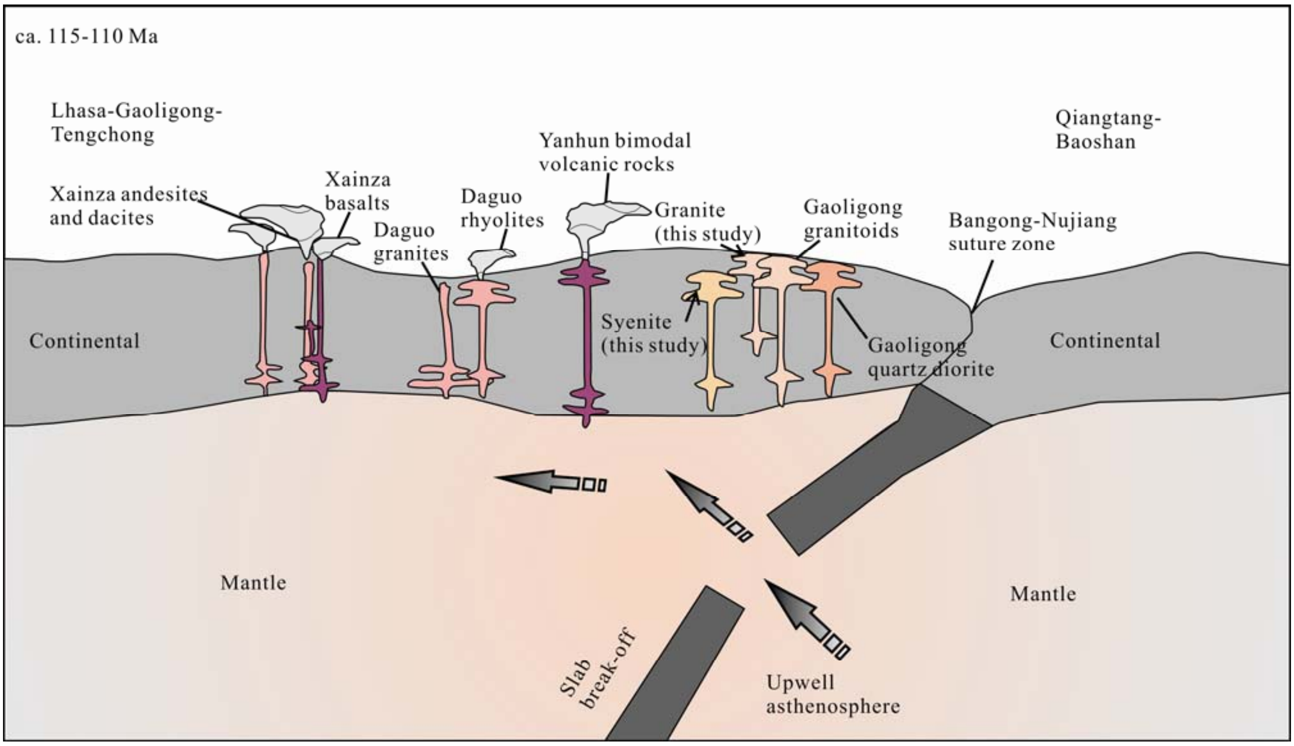


Fig. 12. Diagram of schematic illustration for the late Early-Cretaceous magmatisms (ca. 115–110 Ma) from Lhasa to Gaoligong (after Chen et al., 2014 and Zhu et al., 2017b).

and granites emplaced at ca. 115.3±0.9 Ma and ca. 115.7±0.8 Ma.

(2) Geochemical, isotopic and in-situ zircon Hf isotopic data show that the syenites were possibly derived from mixing of mafic lower crustal and evolved sediments-derived materials, and the fractionation of some ferro-magnesian mineral and plagioclase may occur during the evolution of magma. The granite was derived from the melting of predominated metasedimentary greywackes in the ancient continental crust.

(3) Together with magmatic data in the literatures, we suggest the Early Cretaceous magmatism in the Tengchong block was dominated by magmas generated by the partial melting of ancient crustal material. And ca. 115 Ma syenites and granites are also the products that associated to the slab break-off of subducted Bangong-Nujiang Meso-Tethys oceanic lithosphere.

## Acknowledgements

This work was jointly supported by the National Natural Science Foundation of China (Grant Nos. 41421002, 41190072, 41372067 and 41102037) and the program for Changjiang Scholars and Innovative Research Team in University (Grant IRT1281). Support was also provided by the Foundation for the Author of National Excellent Doctoral Dissertation of PR China (201324), and the MOST Special Fund from the State Key Laboratory of Continental Dynamics, Northwest University, and Province Key Laboratory Construction Item (08JZ62).

Manuscript received Feb. 15, 2017
accepted Sept. 24, 2017
edited by Fei Hongcai

### References

Atherton, M.P., and Petford, N., 1993. Generation of sodium-rich magmas from newly underplated basaltic crust. *Nature*, 362: 144–146.

Bonin, B., 1990. From orogenic to anorogenic settings: evolution of granitoid suites after a major orogenesis. *Geological Journal*, 25: 261–270.

Brown, M., 2013. Granite: from genesis to emplacement. *Geological Society of America Bulletin*, 125(7–8): 1079–1113.

Cao, H.W., Zhang, S.T., Lin, J.Z., Zheng, L., Wu, J.D., and Li, D., 2014. Geology, geochemistry and geochronology of the Jiaojiguanliangzi Fe-polymetallic deposit, Tengchong County, western Yunnan (China): regional tectonic implications. *Journal of Asian Earth Sciences*, 81: 142–152.

Chappell, B.W., and White, A.J.R., 1992. I- and S-type granites in the Lachlan Fold Belt. *Geological Society of America Special Papers*, 272: 1–26.

Chen, S.Z., Xing G.F., Li, Y.N., Xi, W.W., Zhu, X.T., and Zhang, X.D., 2017. Re-recognition of Tieshan "syenite" and its geological significance in Zhenghe, Fujian Province. *Acta Geologica Sinica* (English Edition), 91(S1): 72–73.

Chen, Y., Zhu, D. C., Zhao, Z. D., Meng, F. Y., Wang, Q., Santosh, M., Wang, L.Q., Dong, G.C., and Mo, X.X., 2014. Slab breakoff triggered ca. 113 Ma magmatism around xainza area of the Lhasa terrane, Tibet. *Gondwana Research*, 26(2):

449–463.

Chu, Z.Y., Chen, F.K., Yang, Y.H., and Guo, J.H., 2009. Precise determination of Sm, Nd concentrations and Nd isotopic compositions at the nanogram level in geological samples by thermal ionization mass spectrometry. *Journal of Analytical Atomic Spectrometry*, 24: 1534–1544.

Cong, F., Lin, S.L., Zou, G.F., Li, Z.H., Xie, T., Peng, Z.M., and Liang, T., 2011a. Magma mixing of granites at Lianghe: In-situ zircon analysis for trace elements, U-Pb ages and Hf isotopes. Science China Earth Sciences 54: 1346–1359.

Cong, F., Lin, S.L., Zou, G.F., Xie, T., Li, Z.H., Tang, F.W., and Peng, Z.M., 2011b. Geochronology and petrogenesis for the protolith of biotite plagioclase gneiss at Lianghe, western Yunnan. *Acta Geologica Sinica* (English Edition), 85(4): 870–880.

Dorais, M.J., 1990. Compositional variations in pyroxenes and amphiboles of the Belknap Mountain complex, New Hampshire: evidence for origin of silica-saturated alkaline rocks. American Mineralogist, 75: 1092–1105.

Elliott, T., 2003. Tracers of the slab. In: Eiler, J. (ed.), *Inside the subduction factory*, vol 138. American Geophysical Union, Geophysical Monograph, Washington DC, 23–45.

Frost, B.R., Barnes, C.G., Collins, W.J., Arculus, R.J., Ellis, D.J., and Frost, C.D., 2001. A geochemical classification for granitic rocks. *Journal of Petrology*, 42(11): 2033–2048.

Goolaerts, A., Mattielli, N., de Jong, J., Weis, D., and Scoates, J.S., 2004. Hf and Lu isotopic reference values for the zircon standard 91500 by MC-ICP-MS. *Chemical Geology*, 206: 1–9.

Grimes, C.B., John, B.E., Kelemen, P.B., Mazdab, F.K., Wooden, J.L., Cheadle, M.J., Hanghoj, K., and Schwartz, J.J., 2007, Trace element chemistry of zircons from oceanic crust: A method for distinguishing detrital zircon provenance. *Geology*, 35: 643–646.

Hao, Z.G., Fei, H.C., Hao, Q.Q., and Liu, L., 2015. China's largest granite-type gas field was discovered in Qinghai –The inorganic theory has aroused attention again. *Acta Geologica Sinica* (English Edition), 89(1): 302–303.

Harris, N.B.W., Xu, R.H., Lewis, C.L., and Jin, C., 1988. Plutonic rocks of the 1985 Tibet Geotraverse: Lhasa to Golmud. *Philosophical Transactions of the Royal Society London*, A327: 145–168.

Hoskin, P.W.O., and Schaltegger, U., 2003. The composition of zircon and igneous and metamorphic petrogenesis. *Reviews in Mineralogy and Geochemistry*, 53: 27–62.

Huang, W.L., and Wyllie, P.J., 1975. Melting reaction in the system $NaAlSi_3O_8$-$KalSi_3O_8$-$SiO_2$ to 35 kilobars, dry and with excess water. *Journal of Geology*, 83: 737–748.

Janoušek, V., Finger, F., Roberts, M., Frýda, J., Pin, C., and Dolejš, D., 2004. Deciphering the petrogenesis of deeply buried granites: whole-rock geochemical constraints on the origin of largely undepleted felsic granulites from the Moldanubian zone of the Bohemian massif. *Geological Society of America Special Papers*, 389: 141–159.

Jin, X.C., 1996. Tectono-stratigraphic units in western Yunnan and their counterparts in southeast Asia. *Continent Dynamics*, 1: 123–133.

Johannes, W., and Holtz, F., 1990. Formation and composition of $H_2O$-undersaturated granitic melts. In: Ashworth, J.R., and Brown, M. (eds.), *High-temperature Metamorphism and Crustal Anatexis*. Unwin Hyman, London, 87–104.

Kamber, B.S., and Collerson, K.D., 2000. Role of hidden subducted slabs in mantle depletion. *Chemical Geology*, 166: 241–254.

Li, Z.H., Lin, S.L., Cong, F., Zou, G.F., and Xie, T., 2012. U–Pb dating and Hf isotopic compositions of quartz diorite and monzonitic granite from the Tengchong-Lianghe block, western Yunnan, and its geological implications. *Acta Geology Sinica*, 86(7): 1047–1062 (in Chinese with English abstract).

Lin, I.J., Chung, S.L., Chu, C.H., Lee, H.Y., Gallet, S., Wu, G., Ji, J.Q., Zhang, Y.Q., 2012. Geochemical and Sr–Nd isotopic characteristics of Cretaceous to Paleocene granitoids and volcanic rocks, SE Tibet: petrogenesis and tectonic implications. *Journal of Asian Earth Sciences*, 53(2143): 131–150.

Litvinovsky, B.A., Jahn, B.M., Zanvilevich, A.N., Saunders, A., Poulain, S., Kuzmin, D.V., Reichow, M.K., and Titov, A.V., 2002. Petrogenesis of syenite–granite suites from the Bryansky Complex (Transbaikalia, Russia): implications for the origin of A-type granitoid magmas. *Chemical Geology*, 189: 105–133.

Liu, D., Zhao, Z., Zhu, D.C., Niu, Y., Harrison, T.M., 2014. Zircon xenocrysts in Tibetan ultrapotassic magmas: imaging the deep crust through time. *Geology*, 42(1): 43–46.

Lubala, R.T., Frick, C., Roders, J.H., and Walraven, F., 1994. Petrogenesis of syenites and granites of the Schiel Alkaline complex, Northern Transvaal, South Africa. *Journal of Geology*, 102: 307–309.

Ludwig, K.R., 2003. ISOPLOT 3.0: A Geochronological Toolkit for Microsoft Excel. *Berkeley Geochronology Center Special Publications*, 4.

Luo, G., Jia, X.C., Yang, X.J., Xiong, C.L., Bai, X.Z., Huang, B.X., and Tan, X.L., 2012. LA-ICP-MS zircon U-Pb dating of southern Menglian granite in Tengchong area of western Yunnan Province and its tectonic implications. *Geological Bulletin of China*, 31: 287–296 (in Chinese with English abstract).

Metcalfe, I., 2013. Gondwana dispersion and Asian accretion: tectonic and paleogeography evolution of eastern Tethys. *Journal of Asian Earth Sciences*, 66: 1–33.

Miller, C., Schuster, R., Kotzli, U., Frank, W.， Purtscheller, F., 1999. Post-collisional potassic and ultrapotassic magmatism in SW Tibet: geochemical and Sr-Nd-Pb-O isotopic constraints for mantle source characteristics and petrogenesis. *Journal of Petrology*, 40: 1399–1424.

Patiňo-Douce, A.E., 1999. What do experiments tell us about the relative contributions of crust and mantle to the origin of the granitic magmas. *Geology society of London*, 168: 55–75.

Qi, L., Hu J., and Gregoire, D.C., 2000. Determination of trace elements in granites by inductively coupled plasma mass spectrometry. *Talanta*, 51: 507–513.

Qi, X.X., Zhu, L.H., Hu, Z.C., and Li, Z.Q., 2011. Zircon SHRIMP U–Pb dating and Lu–Hf isotopic composition for Early Cretaceous plutonic rocks in Tengchong block, southeastern Tibet, and its tectonic implications. *Acta Petrologica Sinica*, 27: 3409–3421 (in Chinese with English abstract).

Qu, X.M., Wang, R.J., Xin, H.B., Jiang, J.H., and Chen, H., 2012. Age and petrogenesis of A-type granites in the middle segment of the Bangonghu-Nujiang suture, Tibetan plateau. *Lithos*, 146: 264–275.

Riishuus, M.S., Peate, D.W., Tegner, C., Wilson, J.R., Brooks, C.K., and Waight, T.E., 2005. Petrogenesis of syenites at a rifted continental margin: origin, contamination and interaction of alkaline mafic and felsic magmas in the Astrophyllite Bay Complex, East Greenland. *Contributions to Mineralogy and Petrology*, 149: 350–371.

Sheppard, S., 1995. Hybridization of shoshonitic lamprophyre and calc-alkaline granite magma in the Early Proterozoic Mt. Bundey igneous suite, Northern Territory. *Australian Journal of Earth Sciences*, 42: 173–185.

Song, S.G., Niu, Y.L.,Wei, C.J., Ji, J.Q., and Su, L., 2010. Metamorphism, anatexis, zircon ages and tectonic evolution of the Gongshan block in the northern Indochina continent—an eastern extension of the Lhasa Block. *Lithos*, 120: 327–346.

Sui, Q. L., Wang, Q., Zhu, D. C., Zhao, Z. D., Chen, Y., Santosh, M., Hu, Z.C., Yuan, H.L., and Mo, X.X., 2013. Compositional diversity of ca. 110 ma magmatism in the northern Lhasa Terrane, Tibet: implications for the magmatic origin and crustal growth in a continent–continent collision zone. *Lithos*, 168–169(3): 144–159.

Sun, S.S., and McDonough, W.F., 1989. Chemical and isotopic systematics of oceanic basalts: implications or mantle composition and processes. *Geological Society, London, Special Publications*, 42(1): 313–345.

Sylvester, P.J.,1989. Post-collisional alkaline granites. *Journal of Geology*, 97: 261–280.

Sylvester, P.J., 1998. Postcollisional strongly peraluminous granites. *Lithos*, 45: 29–44.

Wang, E., and Burchfiel, B., 1997. Interpretation of Cenozoic tectonics in the right-lateral accommodation zone between the Ailao Shan shear zone and the eastern Himalayan syntaxis. *International Geology Review*, 39: 191–219.

Wang, Y.J., Xing, X.W., Cawood, P.A., Lai, S.C., Xia, X.P., Fan, W.M., Liu, H.C., and Zhang, F.F., 2013. Petrogenesis of early Paleozoic peraluminous granite in the Sibumasu Block of SW Yunnan and diachronous accretionary orogenesis along the northern margin of Gondwana. *Lithos*, 182: 67–85.

Wu, F.Y., Liu, Z.C., Liu, X.C., and Ji, W.Q., 2015. Himalayan leucogranite: Petrogenesis and implications to orogenesis and plateau uplift. *Acta Petrolohica Sinia*, 31(1): 1–36.

Xie, J.C., Zhu, D.C., Dong, G., Zhao, Z.D., Wang, Q.and Mo, X., 2016. Linking the tengchong terrane in SW Yunnan with the Lhasa terrane in southern Tibet through magmatic correlation. *Gondwana Research*, 39: 217–229.

Xie, T., Lin, S.L., Cong, F., Li, Z.H., Zou, G.F., Li, J.M., and Liang, T., 2010. LA-ICP-MS zircon U-Pb dating for K-feldspar granites in Lianghe region, western Yunnnan and its geological significance. *Geotectonica et Metallogenia*, 34: 419–428 (in Chinese with English abstract).

Xu, R., Scharer, U., and Allègre, C.J., 1985. Magmatism and metamorphism in the Lhasa Block (Tibet): a geochronological study. *Journal of Geology*, 93: 41–57.

Xu, Y.G., Yang, Q.J., Lan, J.B., Luo, Z.Y., Huang, X.L., Shi, Y.R., and Xie, L.W., 2012. Temporal-spatial distribution and tectonic implications of the batholiths in the Gaoligong-Tengliang-Yingjiang area, western Yunnan: Constraints from zircon U-Pb ages and Hf isotopes. *Journal of Asian Earth Sciences*, 53: 151–175.

YBGMR, (Yunnan Bureau Geological Mineral Resource), 1991. Regional geology of Yunnan Province. Beijing: Geology Publication House, 1–729 (in Chinese with English abstract).

Yan M, Zhang D, Fang X, Ren, H.D., Zhang, W.L., Zan, J.B., Song, C.H., Zhang, T., 2016. Paleomagnetic data bearing on the Mesozoic deformation of the Qiangtang Block: Implications for the evolution of the Paleo- and Meso-Tethys. *Gondwana Research*, 39: 292–316.

Yang, J.H., Sun, J.F., Zhang, M., Wu, F.Y., and Wilde, S.A., 2012. Petrogenesis of silica-saturated and silica-undersaturated syenites in the northern north china craton related to post-collisional and intraplate extension. *Chemical Geology*, 328(11): 149–167.

Yang, J.H., Wu, F.Y., Wilde, S.A., Xie, L.W., Yang, Y.H., and Liu, X.M., 2007. Tracing magma mixing in granite genesis: in -situ U-Pb dating and Hf-isotope analysis of zircons. *Contribution to Mineral and Petrology*, 135: 177–190.

Yang, J.H., Chung, S.L., Wilde, S.A., Wu, F.Y., Chu, M.F., Lo, C.H., and Fan, H.R., 2005. Petrogenesis of post-orogenic syenites in the Sulu Orogenic Belt, East China: geochronological, geochemical and Nd–Sr isotopic evidence. *Chemical Geology*, 214: 99–125.

Yang, J.H., Wu, F.Y., Wilde, S.A., Chen, F., Liu, X.M., and Xie, L.W., 2008a. Petrogenesis of an Alkali syenite–granite–rhyolite suite in the Yanshan Fold and Thrust Belt, Eastern North China Craton: geochronological, geochemical and Nd–Sr–Hf isotopic evidence for lithospheric thinning. *Journal of Petrology*, 49: 315–351.

Yang, Q.J., Xu, Y.G., Huang, X.L., and Luo, Z.Y., 2006. Geochronology and geochemistry granites in the Gaoligong tectonic belt, western Yunnan, tectonic implications. *Acta Petrologica Sinica*, 22: 817–834 (in Chinese with English abstract).

Yuan, H.L., Gao, S., Liu, X.M., Li, H.M., Gunther, D., and Wu, F.Y., 2004. Accurate U-Pb age and trace element determinations of zircon by laser ablation-inductively coupled plasma mass spectrometry. *Geo-standard Newsletters*, 28: 353–370.

Zhang, B., Zhang, J., Zhong, D., Yang, L., Yue, Y., and Yan S., 2012. Polystage deformation of the Gaoligong metamorphic zone: structures, $^{40}Ar/^{39}Ar$ mica ages, and tectonic implications. *Journal of Structural Geology*, 37: 1-18.

Zhang, L., Yang, J., and Zhang, J., 2015. Geochronology and geochemistry of Zengga Mesozoic grantoids from East Gangdese batholith, implications for the re-melting mechanism of granite Formation. *Acta Geologica Sinica* (English Editioin), 89(A02): 113–114.

Zheng, Y.F., Zhang, S.B., Zhao, Z.F., Wu, Y.B., Li, X., Li, Z., and Wu, F.Y., 2007. Contrasting zircon Hf and O isotopes in the two episodes of Neoproterozoic granitoids in South China: implications for growth and reworking of continental crust. *Lithos*, 96: 127–150.

Zhong, D.L, 1998. Paleo-Tethyan orogenic belt in the western parts of the Sichuan and Yunnan Provinces. *Beijing: Science Press*, 1–231.

Zhong, D.L., 2000. Paleotethys Sides in West Yunnan and Sichuan, China. *Beijing: Science Press,* 1–248 (in Chinese with English abstract).

Zhu, D.C., Li, S.M., Cawood, P.A., Wang, Q., Zhao, Z.D., and Liu, S.A., 2015a. Assembly of the lhasa and qiangtang terranes in central tibet by divergent double subduction. *Lithos*, 245: 7–17.

Zhu, D.C., Mo, X.X., Niu, Y.L., Zhao, Z.D., Wang L.Q., and Liu Y.S., and Wu F.Y., 2009. Geochemical investigation of Early

Cretaceous igneous rocks along an east-west traverse throughout the central Lhasa Terrane, Tibet. *Chemical Geology*, 268: 298–312.

Zhu, D.C., Zhao, Z.D., Niu, Y.L., Mo, X.X., Chung, S.L., Hou, Z.Q., Wang, L.Q., and Wu, F.Y., 2011. The Lhasa Terrane: Record of a microcontinent and its histories of drift and growth. *Earth and Planetary Science Letters*, 301: 241–255.

Zhu, D.C., Zhao, Z.D., Niu, Y.L., Dilek, Y., Hou, Z.Q., and Mo, X.X., 2013. The origin and pre-Cenozoic evolution of the Tibetan Plateau. *Gondwana Research*, 23: 1429–1454.

Zhu, R.Z., Lai, S.C., Qin, J.F., and Zhao, S.W., 2015b. Early Cretaceous highly fractionated I–type granites from the northern Tengchong block, western Yunnan: Petrogenesis and tectonic implications. *Journal of Asian Earth Sciences*, 100: 145–163.

Zhu, R.Z., Lai, S.C., Santosh, M., Qin, J.F., Zhao, S.W., 2017a. Early Cretaceous Na-rich granitoids and their enclaves in the Tengchong Block, SW China: Magmatism in relation to subduction of the Bangong-Nujiang Tethys ocean. *Lithos*, 286: 175–190.

Zhu, R.Z., Lai, S.C., Qin, J.F., Zhao, S.W., 2017b. Late Early-Cretaceous quartz diorite-granodiorite-monzogranite association from the Gaoligong belt, southeastern Tibet Plateau: Chemical variations and geodynamic implications. *Lithos*, 288: 311–325.

## About the first author

ZHU Renzhi, male; born in 1989 in Mei County, Shaanxi Province; PhD; graduated from Northwestern University; State Key Laboratory of Continental Dynamics, Department of Geology, Northwest University. He is now interested in the study on petrology and geochemistry. Email: rzzhunwu@163.com; phone: 029-88307610, 18729017556.